Chapter 4
Amphiphilic Janus Particles at Interfaces

Andrei Honciuc

Acronyms

3-TSPM	3-(trimethoxysilyl)propyl methacrylate
APS	(3-Aminopropyl)triethoxysilane
CA	contact angle
DIW	de-ionised water
HLB	hydrophilic–lyophilic balance
HP	homogeneous particle
IBA	isobornyl acrylate
IFT	interfacial tension
JP	Janus particle
MMA	methyl methacrylate
NP	nanoparticle
OTS	n-octadecyltrichlorosilane
P(3-TSPM)	poly(3-(trimethoxysilyl)propyl methacrylate)
PA	polyacrylate
PAA	poly(acrylic acid)
PI	polyisoprene
PMMA	poly(methyl methacrylate)
pNA	poly[N-isopropylacrylamide-co-(acrylic acid)]
PPA	poly(propargyl-acrylate)
PPFBEM	poly(2-(perfluorobutyl)ethyl methacrylate)
PPy	polypyrrole
PS	polystyrene

A. Honciuc (✉)
Institute of Chemistry and Biotechnology, Zurich University of Applied Sciences, Waedenswil, Switzerland
e-mail: andrei.honciuc@zhaw.ch

PS-PDIPAEMA   polystyrene-poly[2-(diisopropylamino)ethyl methacrylate
PtBA   poly(tert-butyl acrylate)

4.1   Introduction

Janus particles (JPs) can be generally defined as asymmetric particles with at least two surface regions or bulk composition differing in their physicochemical properties. JPs can adopt different shapes, for example, perfectly spherical with two hemispheres having different surface properties as depicted in Fig. 4.1, or they can adopt different shapes, such as snowman [1], or dumbbell, hybridised-like [2] orbitals, mushroom [3] with clear geometrical and topological asymmetries. Under the same "Janus" category other particles, such as raspberry, [4] rods or discs [5] have also been included and generally all asymmetric particles, as long as there is a difference in composition or surface properties on the same particle but on distinctive regions. Probably the most typical shape of a Janus particle is that of a dumbbell or snowman, Fig. 4.1. Unlike homogeneous particles (HPs) the JPs have some interesting properties and exhibit extra-functionality conferred by their asymmetry. One example of such functionality is amphiphilicity. Due to the inherent polarity contrast between two surface regions, they resemble surfactants with one polar side and one-less polar; therefore, the JPs are promising as "solid
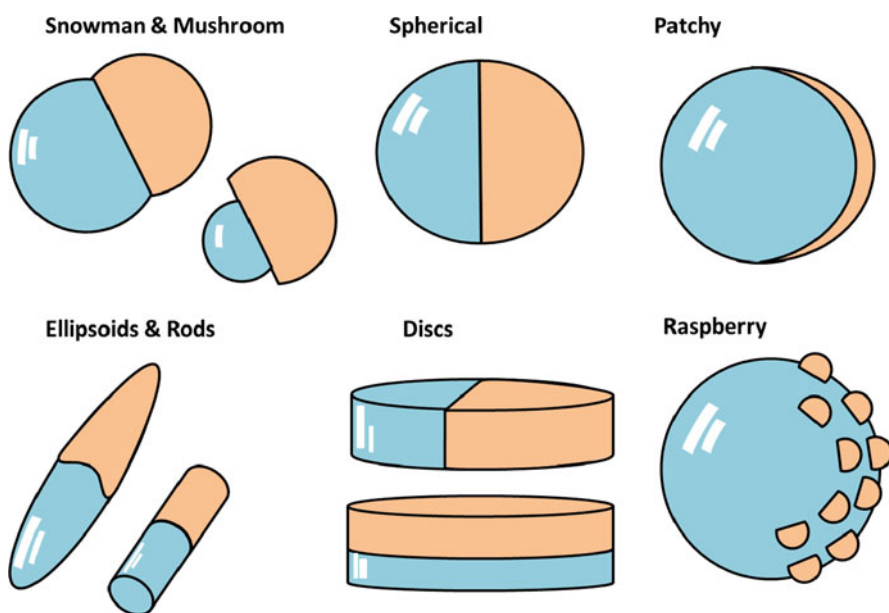

Fig. 4.1   Types of Janus particles

state amphiphiles" or the next generation of amphiphiles. But unlike surfactants, generally small molecules, or low molecular weight polymers, JPs exhibit some significant differences. First, because they are solid-state particles and due to their size, they have large interfacial attachment energies, on the order of thousands of kT (parameter that scales with the R^2, where R is the radius of the particle), meaning that once adsorbed at the interface they remain trapped and secondly their diffusion through the liquid is much slower. This can be an advantage because JPs can be used as emulsifiers of oils and water and create ultrastable Pickering emulsions. Pickering emulsions can also be generated with HPs but it has been shown that due to their amphiphilicity the JPs are several times more interfacially active and thus superior in such applications. Furthermore, the JPs are also active at the air–water interface and this makes them attractive as stabilisers of air bubbles and foams. Their size may also bring further advantages, for example, they can be used as carriers of actives (small molecules serving as pharmaceutically active ingredients), or smart catalysts moving in concentration gradients and even nanomotors for transportation of "heavy" cargo, which molecular surfactants cannot do. JPs can also be regarded as building blocks of matter that can self-assemble to give rise to suprastructures. JPs can be multifunctional because they can carry different properties on each lobe; this is especially attractive to creating new multifunctional materials where the surface and bulk-like properties can be combined to obtain unexpected functionalities. For example, it has been demonstrated that conductivity and surface polarity of snowman-type JPs can be tuned by changing the lobe ratio between a semiconductive lobe and an electrically insulating lobe [6]. This opens up the path to new multifunctional materials made from Janus building block that carry on the different lobes different functionalities, optic, magnetic, surface functional groups, etc.

4.2   Short History of Asymmetric Janus Particles

Janus particles have a relatively short history and only came recently into existence through the imagination of a handful of scientists in the late 1980s. The concept of an asymmetric and amphiphilic particle was put forward by Casagrande, Veysié and de Gennes. The first synthesis of micron-sized JPs was attributed to the former two authors, while de Gennes baptised them after the Roman god Janus. Janus was the two-faced god of transitions, gates, passages and new beginnings, after which the month of January was named. Janus is a god in Roman mythology and was considered to be the most important one because it provided passage to the other gods. Janus is often depicted with two faces of an old man, but initially this was depicted with the face of young man looking back and old man looking forward, very suggestive of the time passage. In his famous Nobel Prize talk [7] de Gennes also called the asymmetric particle Janus grains. Interestingly, the amphiphilic nature of the Janus glass beads produced by Casagrande et al. [8] could be probed directly for the first time by observing from photographs of

breath-patterns "figures de soufflé" clearly showing droplets of water pearling up on the hydrophobic side but making a contiguous film on the hydrophilic side. A few years earlier, in 1985, Grünning et al. [9] filed a patent claiming a procedure for the preparation of amphiphilic particles from 100 μm hollow beads, with the exterior surface hydrophobised and hydrophilic side remaining in the interior, which were then crushed to produce irregularly shaped glass shards that were amphiphilic; this procedure was later detailed by one of the inventors, Rosmmy in 1998 [10]. Remarkably, right from the beginning the inventors proposed the use of such particles as surface active products, for emulsification, production of foams and deployment in tertiary oil recovery. This was the first time when amphiphilic particles were produced in large amounts. In 1991 Chen et al. [11] synthesised biphasic snowman type polymeric particles by seeded emulsion polymerisation and phase separation, but were probably unaware of the fact that they synthesised the first polymeric JPs. Within the 1990s to 2000s the scientific community did not seem to catch interest in these particles. It was then only much later, in the early of the first decade of the twenty-first century when the new synthetic routes were published. This was in part triggered by the theoretical work of Ondarçuhu [12] and later by Binks and Fletcher [13] who showed by calculation that the interfacial activity of spherical JPs at their maximum amphiphilicity (highest polarity contrast), in terms of interfacial desorption energy should be up to three times larger than that of HPs and much larger for snowman or dumbbell JPs. However, the desorption energy only is not a proper gauge for measuring the interfacial activity, but rather the ability to lower the interfacial tension, as it will be discussed later. Since then the research on Janus particles grew exponentially, estimated from the increasing number of publications each year. Initially the JPs could only be produced in very low amounts and the synthetic challenges were preventing their use in applications. Currently JPs can be produced in large amounts and therefore, their use in new applications is being explored, such as emulsifiers, catalysts, foam stabilisers, polymer blend compatibilisers, amphiphiles, building-blocks, etc. It turns out the Janus is not only reserved for synthetic particles but also naturally occurring proteins, such as the hydrophobins produced by fungi, HFBII from *Trichoderma Reesei* that is nearly globular with a 3 nm diameter and 7.2 kDa [14]. Interestingly, it has been shown that HFBII is an excellent foam stabiliser and is responsible for beer gushing. Beer gushing is the phenomenon of beer foam gushing out of the bottle when opened or mechanically shocked by hitting its bottom to the table, completely emptying the bottle [15]. The HFBII ends up in malt by fungi infection.

4.3 General Synthetic Routes

JNPs can be prepared by chemical or physical methods. Next we give a short overview of the methods used in the synthesis of JPs.

4.3.1   Masking and Asymmetric Modification

This preparation method relies on a simple concept, in a first step one side of a spherical particle is masked by a protective layer and in a second step chemical or physical modification is performed on the unmasked part followed by the removal of the masking layer. In this way the original HP particle is now a JP particle because it has different surface properties, even though its bulk composition remains the same. While the concept of the method is simple its implementation and scalability can be an issue. The masking and modification method was first used by Casagrande et al. [8] who used varnish to mask half of the micron-sized spherical glass beads and performed silanisation/hydrophobisation on the other half of the spherical bead to produce JPs. Instead of applying a varnish, a spherical particle can be deposited on a flat surface or self-assembled in a monolayer followed by the deposition, via evaporation, of a metal on the exposed part, Fig. 4.2. Due to the masking, the metal will only deposit on one side of the particle facing away from the flat substrate. In this way hybrid polymer/metallic, silica/metallic JPs can be made. This is a highly effective method to produce JPs with tunable optical or electric properties as the thickness of the metal layer deposited can be precisely controlled; Kawaguchi et al. [16] applied this method to produce JPs with a functional gold surface for control of surface plasmon resonance and thus the colour of the particles with potential applications in paper displays. Other patchy JPs with tunable optical properties were successfully prepared by Composto et al. [17]. Bimetallic Co/Ni Ag/Au, Ni/Au Janus particles could be made using the same method by Carroll et al. [18] from a single layer of self-assembled silica beads on a substrate in two steps:
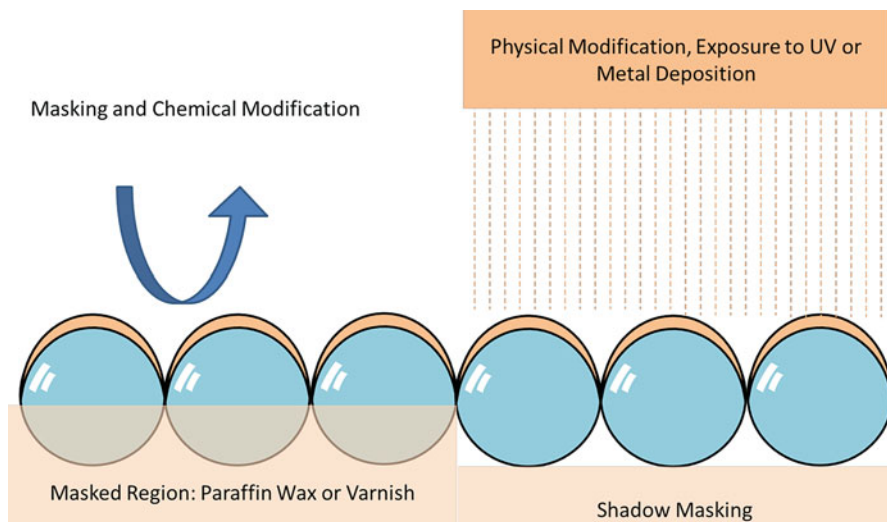

Fig. 4.2   Masking and surface modification techniques for manufacturing of Janus particles

first the particles were coated with one metal using e-beam evaporation, then the beads were inverted and coated with another metal. The preparation of JPs from 2D layers is highly effective but not scalable to produce large amounts. In this context Granick's group [19, 20] has succeeded in producing gram-scale amount of JPs by first taking fused silica particles HPs (800 nm and 1.5 µm in diameter) and use them to emulsify molten wax at high temperature. Then the obtained o/w emulsion was cooled to room temperature to obtain solid wax colloidosomes that have HPs trapped/embedded on their surface. Because the HPs were half protected by the wax they could be chemically reacted with APS on the water exposed part, then after dissolving the wax colloidosome they could be hydrophobised on the other side with OTS. In this way gram-scale amounts of JPs could be obtained. Suzuki et al. [21] used the same strategy to prepare large amounts of JPs from thermo-responsive pNA microgels by first trapping them at the heptane/water via emulsification to create o/w Pickering emulsions. Once at the interface of the oil droplets the microgel particles were further reacted with water soluble only ethylenediamine (ED) and 1-ethyl-3-(3-dimethylaminopropyl)-carbodiimide hydrochloride (EDC) and amine groups were introduced this way at the surface of the water exposed gel particles. Smaller Au nanoparticles could be attached only on the -NH$_2$ rich side of the stimuli-responsive Janus microgel particles. Fujimoto et al. [22] prepared Janus microspheres at the solid–liquid interface by allowing poly(methacrylic acid-co-nitrophenyl acrylate) microspheres to interact with a substrate on which human immunoglobulin (IgG) was previously adsorbed. After the microspheres settled on the flat substrate, NaOH was added to activate the ester bonds by cleaving the p-nitrophenol. The part of the microsphere touching the IgG-substrate reacted with the amine and thiol bonds of the IgG molecule, while the other side remained unmodified.

4.3.2 Seeded Emulsion Polymerisation and Phase Separation

The preparation of JPs by seeded emulsion polymerisation and phase separation of polymers was first performed by Chen et al. [11] in 1991, although probably unaware of the fact that these were being baptised Janus particles by P. de Gennes in the same year. The procedure is simple in theory, and starts with monodisperse seed latex polystyrene (PS) particles. Their methods were later revived and extended to a multitude of different biphasic polymeric Janus particles. The method consists of first preparing polymeric latex particles in the nanometre range, such as PS. Then these are re-dispersed in water and a second monomer (partially soluble in water) is added, such as MMA or 3-TSPM. Emulsification of the monomers is necessary for the swelling of the latex particles to succeed. Then the mixture is given some time for the swelling of the seed particle by the monomer to take place, eventually the polymerisation is started. As the monomer polymerises the newly created polymer, due to incompatibility with PS, bulges out from the seed particles leading to the creation of a second lobe and the formation of snowman
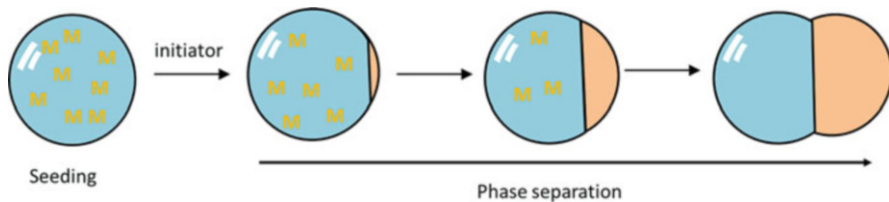
Fig. 4.3 Cartoon depicting the preparation of JPs via seeded emulsion polymerisation and phase separation method. The second lobe grows as the monomer (M) from the reservoir is being consumed

or dumbbell type biphasic Janus particles as depicted in Fig. 4.3. The degree of phase separation as well as the final geometry of the obtained JPs depends on the Flory–Huggins interaction parameter, wettability between the two polymers, crosslinking degree, phase separation kinetics. Wettability between the polymers can also be influenced by initiator type, addition of surfactant, etc. [11]. Several different types of polymeric JPs could be made this way and with precisely tuned reaction conditions snowman-type particles could be produced. JPs with hard and soft lobes PtBA/PS JPs were prepared by Bon et al. [23], Daeyeon Lee et al. [24] prepared PS/PPA JPs that can be subsequently modified via thiol-yne click reactions, Sun et al. [25] obtained PS/PMMA with a hollow PS lobe, Hoffmann et al. [26] prepared PMMA/PS JPs from PMMA seeds, Weitz et al. [27] synthesised PS/PMMA and PS/PtBA seeds. Note the convention we have used, the initial seed particles are first written followed by the second lobe.

4.3.3 Microfluidic and Capillary Electro-Jetting Methods

Multi-compartmented or multiphasic particles can be fabricated by microfluidic as well as electro-jetting processes [28]. Droplet microfluidics refer to the preparation and manipulation of discrete micron-sized droplets, double emulsions droplets, microbubbles, etc., and the fabrication of polymeric JP by this method has been extensively reviewed [29]. Black and white bicolored JPs with electrical anisotropy were synthesised for the first time by Torii et al. [30] using a microfluidic co-flow system. Pigments of carbon black and titanium oxide were dispersed in IBA then were separately introduced into the Y-junction at the same volumetric flow rate to form a two-colour stream followed by break-up into droplets due to surface tension further down into the stream channel. The obtained Janus droplets were polymerised outside of the microfluidic system by heating, but in principle polymerisation can also be done in the microfluidic channel by UV exposure. Multicoloured JPs with electrical anisotropy can be used in panel displays where the colour switch can be done by changing the orientation of the JPs and this can be actuated between two electrodes by applying voltage.

The electrodynamic co-jetting methods consist of flowing two or more different polymer solutions through a bi-compartmented metal capillary, while maintaining a laminar flow, at the apex of the capillary tip the polymer solution comes together to form a droplet to which a high electrical voltage is applied. The application of the electric field causes the solutions to form a Taylor cone, which creates a spray of individual droplets accelerating toward the counter electrode. During this, the solvents from the droplet evaporate, resulting in polymeric nanoparticles that are collected on the surface of the counter electrode. In this method due to the rapid evaporation of the solvents, and because the process is very fast, the polymers touching do not have sufficient time to mix, the resulting nanoparticles remain bi-compartmented. These methods have the great advantage of high-throughput to prepare large amounts of micrometre sized multiphasic Janus particles. Preparing of monodispersed nano-sized particle is more challenging; however, Lahann et al. [31] succeeded with the synthesis of PMMA/PtBMA biphasic Janus nanoparticles having diameters $d = 172 \pm 28$ nm and tri-phasic [32] from poly(ethylene oxide), poly(acrylic acid) and poly(acrylamide-*co*-acrylic acid). Furthermore the individual polymer phases can be independently loaded with biomolecules or selectively modified with model ligands [33]. The resulting JPs are generally non-crosslinked, but it is possible to crosslink these by using a photoinitiator and by UV exposure after immediate generation of the oil droplets can lead to cross-linking of the polymers [34].

4.3.4   Polymer Co-precipitation and Phase Separation

One of the most simple and feasible pathways to synthesise JPs is the phase separation of polymeric solutions, such as A/B homopolymer/homopolymer and AB/C copolymer/homopolymer blends dissolved under confinement followed by the evaporation of the solvent. This method usually involves an oil-in-water (o/w) emulsion system working as the confinement system, in which oil droplets comprise two incompatible polymers with a large Flory–Huggins interaction parameter, such as PS and PMMA, dissolved in a common solvent [35]. After evaporation, the solvent leaves behind solid well-defined particles, with the two separated polymer phases inside. Deng et al. [36] were able to prepare JPs with hierarchical structures from AB/C polymer blends. The preparation of polymeric Janus nanoparticles by this method involves first dissolving multiple, chemically distinct polymers in a mutually favourable solvent and gradually altering the solubility character of the solution until the polymer molecules co-precipitate as particles and different polymers phase separate. Priestley et al. [37] succeeded in scaling up preparation of JPs and multi-compartmented particles by co-precipitation and phase separation method from dissimilar polymers to up to 1400 kg/day by designing a so-called confined impinging jet mixer, a technique they called termed flash nanoprecipitation (FNP). In the FNP method, the PS and PI (with a Flory–Huggins interaction parameter $\chi_{PS\text{-}PI} = 0.07$) were dissolved at a certain ratio in a common solvent

THF and injected in one of the arms of a fluidic device, in the same time the "anti-solvent", DIW, was flown through a second arm of a fluidic device. The two arms converged into a single one called the mixing region where the PI-PS co-precipitated and phase separated as the solvent rapidly exchanges with an "anti-solvent". By changing the polymer feed concentration from 0.1 to 1.0 mg/mL they could systematically increase the size of the Janus nanocolloids from ≃125 to 540 nm in diameter. Anisotropy of the produced particles could also be changed by altering the PS–PI polymer ratio from 1:4 to 4:1 to produce multifaceted colloids. The later technology proves to be highly versatile, with perhaps the only disadvantage is that starting already from polymer chains the co-precipitation and phase separation methods do not offer the possibility for polymer cross-linking restricting the use of the obtained JPs, for example, as stabilisers in Pickering emulsions in which case the JPs would likely disintegrate/dissolve upon interaction with the oil.

4.4   Tuning the Surface Polarity in JPs

Unlike the HPs whose surface polarity can be changed only by chemical means, tuning the surface polarity of the JPs can be done in a gradual and predictive way by adjusting the geometric ratio or the surface area between the lobes having different polarities. In this way, homologous series of JPs can be created, in analogy to homologous series of molecular surfactants, for example, by increasing the amount of the monomer to seed latex particles in seeded emulsion polymerisation, Fig. 4.4.

Wu and Honciuc [1] have synthesised a homologous series of PS/P(3-TSPM) JPs by changing the volume of 3-TSPM monomer to the PS seed NPs, see Fig. 4.4, and demonstrated that the PS lobe is the less polar than the P(3-TSPM) one; by increasing the size of the more polar P(3-TSPM) they could achieve polarity inversion in the homologous series purely by geometric means when the size of the P(3-TSPM) became larger than that of the PS lobe. The polarity inversion in the homologous series could be demonstrated from heptane–water emulsification experiments, whereas the JPs with smallest P(3-TSPM) lobe have high affinity to heptane, the largest P(3-TSPM) lobe JPs have higher affinity to water and as a consequence an inversion of the emulsion phase from w/o to o/w occurs at the middle of the homologous series. But the aspect ratio and implicitly the polarity of the JPs can also be tuned dynamically by stimuli, such as in stimuli-responsive particles that change both their geometry and polarity. One such example are the shape-changing and pH-responsive particles PtBA/PS produced in Lee's group [38] which upon cleaving the -tBA group by hydrolysis in the PtBA lobe, pH-responsive PA/PS JPs are obtained. At high pH the carboxyl groups are mostly ionised, resulting in large intake of water and swelling of the PA lobe; as a consequence, the particles become polar, have a good affinity to water and form o/w emulsions. At low pH, below the pKa value, the -COOH groups are protonated, non-ionic and
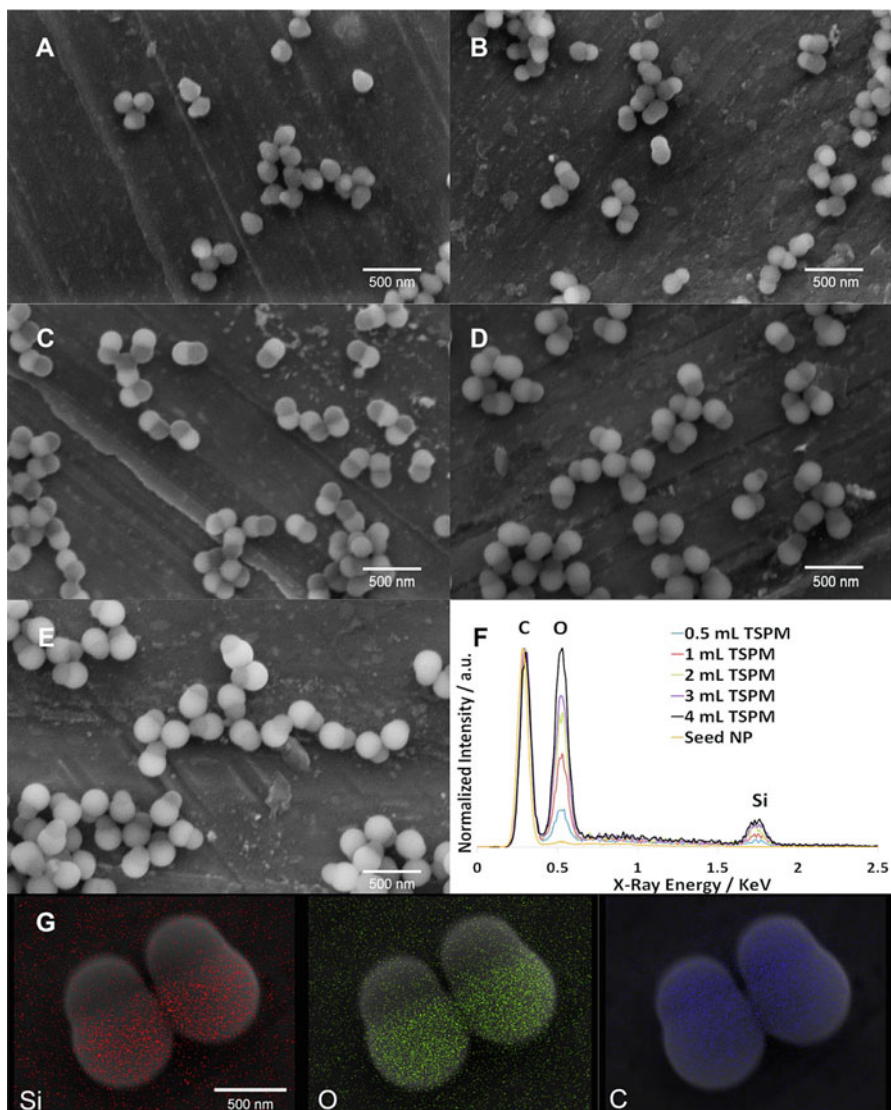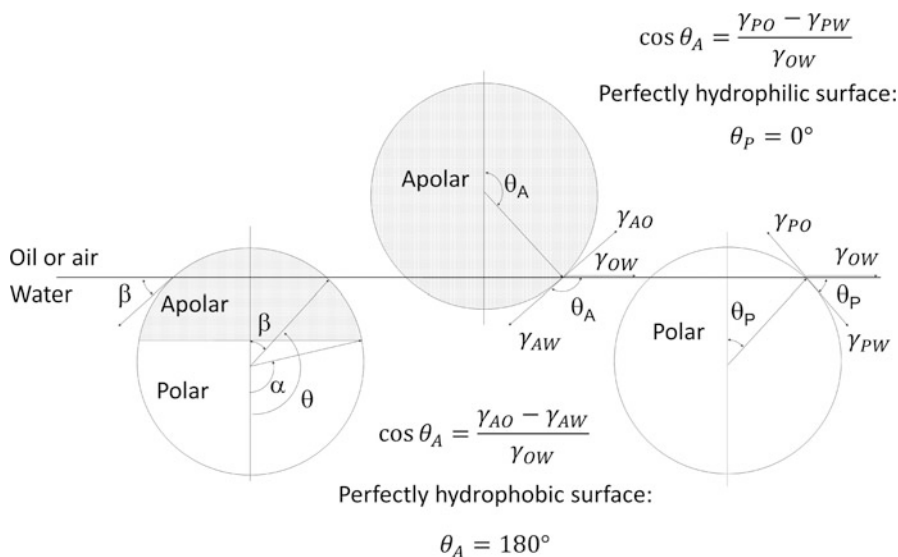
Fig. 4.4 SEM images of PS/P(3-TSPM) JPs with progressively enlarged P(3-TSPM) lobe (light-grey/white) from the same seed PS NPs (dark-grey). (**a**)–(**e**) JPs with progressively larger lobes obtained for a volume of 3-TSPM monomer (**a**) 0.5 mL, (**b**) 1 mL, (**c**) 2 mL, (**d**) 3 mL and (**e**) 4 mL added to 1 g of PS seed NPs; (**f**) EDX spectra, normalised with respect to the reference carbon peak of the PS seed NPs. (**g**) EDX mapping of "2 mL TSPM" JNPs obtained from larger seed PS NPs, 320 ± 5 nm diameter, showing asymmetric distribution of oxygen, silicon elements, namely a higher concentration in the P(3-TSPM) lobe in contrast to a symmetric distribution of carbon in both Janus lobes. Reprinted with permission from Ref. [1]. Copyright 2016 American Chemical Society

there is no water intake of the lobe; the geometry of the lobe remains rigid and the particles have higher affinity to the oil phase forming w/o emulsions.

Surface Polarity Contrast Between Lobes: Quantification of Amphiphilicity
The JPs are amphiphilic because of the inherent surface polarity contrast between the lobes. The concept of amphiphilicity is however understood in a qualitative way and it denotes the ability of the amphiphile to adsorb and partition at the oil/water or air/water interfaces.

The earlier theoretical work of Ondarçuhu [12] already set the framework for estimating the amphiphilicity balance of spherical JP adsorbed at an interface (oil–water or air–water) by measuring its contact angle with reference to one of the phases, usually the water phase. His geometrical model was parameterised as to include the angle α that denotes the position of the boundary between the apolar and polar regions of the Janus lobes, see Fig. 4.5. The contact angle of the JP with the interface is given by β. For a perfectly spherical JP α is almost a measure of its amphiphilicity, because zero amphiphilicity (corresponding to homogeneous particles) corresponds to either $\alpha = 0$ or $180°$. Strongest amphiphilicity is expected when $\alpha = 90°$. Two additional parameters were introduced, namely θ_A and θ_P which are the contact angle of one of the phases (depends on the chosen reference but typically water is taken as a reference) with each of the lobes, the apolar and

$$\cos \theta_A = \frac{\gamma_{PO} - \gamma_{PW}}{\gamma_{OW}}$$

Perfectly hydrophilic surface:
$$\theta_P = 0°$$

$$\cos \theta_A = \frac{\gamma_{AO} - \gamma_{AW}}{\gamma_{OW}}$$

Perfectly hydrophobic surface:
$$\theta_A = 180°$$

Fig. 4.5 Model describing a spherical JP, apolar HP and polar HP at the oil–water interface. The parameters can be defined as follows: α keeps track of the position of the boundary between the apolar and polar regions of the JP, whereas β keeps track of the position of the oil–water interface relative to the particle centre and it represents the contact angle with the water phase. The angle θ_A is the water contact angle of the apolar HP corresponding to the apolar region of the JP, the θ_P is the water contact angle of the HP corresponding to the polar region of the JP

the polar, respectively. These angles can be better understood if HPs corresponding to each of the JP lobes are depicted at the interface as in Fig. 4.5. For JPs no amphiphilicity is expected when $\theta_A - \theta_P = 0°$ and the strongest amphiphilicity for $\theta_A - \theta_P = 180°$, meaning that one lobe has a perfectly hydrophobic surface and the other a perfectly hydrophilic surface, respectively.

Later Jiang and Granick [39] introduced the concept of Janus balance or "J-value" to effectively quantify the amphiphilicity as the dimensionless ratio of work to transfer an amphiphilic JP from the oil–water interface into the oil phase, normalised by the work needed to move it into the water phase:

$$J = \frac{\sin^2 \alpha + 2\cos\theta_P(\cos\alpha - 1)}{\sin^2 \alpha + 2\cos\theta_A(\cos\alpha + 1)}, \tag{4.1}$$

where the angle α, θ_A and θ_P have the same meaning as those depicted in Fig. 4.5. The above equation shows that Janus balance depends on the relative areas of hydrophilic and hydrophobic lobe, quantified by α and on the hydrophobicity of the two sides, quantified by θ_A and θ_P. When θ_A and θ_P are fixed, J increases as α increases (because $\cos\theta_P < 0$) meaning a larger hydrophilic area. When α is fixed, J increases when θ_A and θ_P increase, which corresponds to the hydrophilic part becoming more hydrophilic or the hydrophobic part becoming less hydrophobic. The larger the magnitude of J, the more hydrophilic is the JP, which follows the same trend as that of the HLB[40] for surfactant molecules: larger HLB meaning a higher affinity for water. The J value can be therefore calculated from the interfacial contact angle and the geometry of Janus particles. However, the above model has two caveats: first the model was deduced by assuming a perfect orientation of the particle at the oil/water interface, i.e. the Janus axis perpendicular to the interface, and second it assumed a perfectly spherical particle, but α loses its meaning for a snowman, dumbbell or any other shape of the JP and the problem has to be re-parameterised. Therefore, the above model is not generally applicable. Based on these calculations Binks and Fletcher [13] have shown that the interfacial activity of a JP can be up to three times larger than that of an HP. This is lately taken, mistakenly, as an upper limit of what JPs can achieve but in fact the interfacial activity of these dual particles can be significantly larger than a factor of three for other geometries, as shown in simulations by Gao et al. [41]. However, it would be more useful if amphiphilicity can be discussed quantitatively and can be measured.

In a different approach to quantify the amphiphilicity of any shape of JPs Honciuc et al. [1, 6, 42] have proposed the direct calculation of the HLB balance of a JP using Griffin's approach [43], that is, the same model used to calculate the HLB balance for a homologous series of surfactants [40] and adapted it for JPs:

$$\text{HLB} = 20\frac{A_{\text{Polar}}F_1}{A_{\text{Polar}}F_1 + A_{\text{Apolar}}F_2}, \tag{4.2}$$

where A_{Polar} is the area of the polar lobe, A_{Apolar} is the area of the non-polar lobe and in addition we have introduced the weighting factors F_i ($i = 1, 2$) accounting for the "degree" of polarity of the lobes. The original approach of Griffin for surfactants did not account for the polarity of the surfactant moieties, but only considers their relative molecular weights $20 M_{w(polar)} / M_{w(molecule)}$. The above equation takes the value of 20 for $F_2 = 0$ and 0 for $F_1 = 0$, which are two limiting situations: strongly polar and apolar particles, respectively, with no amphiphilicity. On the other hand a value of $F_1 = 1$ (hypothetical 100% polar surface) and $F_2 = 1$ (hypothetical 100% non-polar surface) assumes an "ideal" polarity contrast between the two surface regions, see Fig. 4.6a, and thus, the HLB is decided by the geometry of the lobes, i.e. their aspect ratio. The polarity weighting factors F can be calculated from the ratio between the polar and apolar or dispersive surface energy components for each of the Janus lobes, as depicted in Fig. 4.6:

$$F_1 = \frac{\gamma_1^p}{\gamma_1^p + \gamma_1^d} \quad \text{and} \quad F_2 = \frac{\gamma_2^d}{\gamma_2^p + \gamma_2^d}, \tag{4.3}$$

where the small Greek gammas are the surface energies and the superscripts "p" and "d" indicate the polar and dispersive or apolar surface energy components of the corresponding Janus lobes, subscripts 1-polar lobe and 2-apolar lobe. In practice, to determine F one must know the surface energy and its polar and dispersive components which is not trivial. Recently, Mihali and Honciuc [6] have measured the surface energy and the polar/disperse components of each Janus lobes in a homologous series of semiconducting PPy/P(3-TSPM) JPs with increasing size of the polar lobe and with these values they have calculated the corresponding weighting factors F and subsequently the HLB values, these are given in Table 4.1.
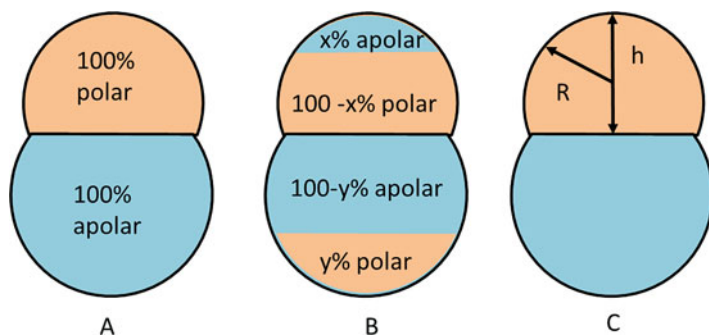
Fig. 4.6 (**a**) Hypothetical amphiphilic dumbbell Janus particle displaying an ideal polarity contrast between a purely dispersive surface and "purely polar" surface of the two Janus lobes, where the polarity factors are $F_1 = F_2 = 1$; (**b**) the more realistic representation of a snowman Janus particle with the surface polarity of the lobes departing from ideality and whose polarity factors, F_1 and F_1 can be calculated with Eq. (4.3); (**c**) the parameters of a JNP used to calculate areas of the lobes, radius R and height of the lobe h

Table 4.1 Aspect ratio and HLB values in the homologous series of JNPs

JPs in increasing order of the (3-TSPM) polar lobe	[a]Area × 1000/nm^2, PPy-lobe	[a]Area × 1000/nm^2, P(3-TSPM)-lobe	Aspect ratio P(3-TSPM) /PPy	[b]HLB number	[c]F_1	[c]F_2	[d]HLB number (weighted)
PPy/P(1 mL 3-TSPM)	177.6	83.2	0.5	6	0.93	0.92	6
PPy/P(2 mL 3-TSPM)	211.8	172.9	0.8	9	0.93	0.92	9
PPy/P(3 mL 3-TSPM)	164.1	318.9	1.9	13	0.93	0.92	13
PPy/P(4 mL 3-TSPM)	152.7	348.7	2.3	14	0.93	0.92	14

[a]The areas of the lobes were calculated from the equation $A = 2\pi Rh$, where h is the height of the Janus lobe and R is its radius, Fig. 4.6c
[b]Values calculated with Eq. (4.2) with $F_1 = F_2 = 1$
[c]F_1 and F_2 were calculated with Eq. (4.2)
[d]Values calculated with Eq. (4.2)
From Ref. [6]. Copyright ©2017 by John Wiley Sons, Inc. Reprinted by permission of John Wiley & Sons, Inc.

Interestingly the HLB values calculated for the JPs excluding the weighting factors, in the 5th column of Table 4.1, are similar with those calculated after taking into account the degree of polarity of the lobes, in the 8th column of Table 4.1. That is because the measured F-values are close to unity and thus the JPs have an almost ideal polarity contrast. Calculating HLB value this way for a homologous series of JPs has the advantage of being able to predict the behaviour of JPs with respect to their ability to act as w/o or o/w emulsifiers, discussed later. HLB range, taking values from 1 to 20, is more readily understood by scientists working with surfactants. For example, amphiphiles with values below 10 on the Griffin's scale are good w/o emulsifiers (good affinity to the oil phase), while those with HLBs above 10 are good o/w emulsifiers, which was clearly shown by the emulsification experiments [1]. We believe this method to quantify the Janus balance is universally applicable because it makes no assumptions about the particle geometry, orientation or its position at interface.

4.5   Interfacial Activity and Adsorption at Interfaces

It is well known that particles can spontaneously adsorb at liquid–liquid and air–liquid interfaces and can thus lower the system's Gibbs free energy, which translates into the reduction of the interfacial IFT. By monitoring the decrease of the interfacial tension with time, i.e. the dynamic surface tension, usually with pendant drop tensiometry, one can obtain information about JPs' interfacial adsorption kinetics. The bulk diffusivity of any particles obeys the Stokes diffusion law. For particles with appropriate wettability the bulk-to-surface diffusion may lead to the adsorption and attachment at the interface if: (a) there is no strong electrostatic repulsion

interaction between the interface and the particle (image charge repulsion) and (b) the energy costs related to the surface dehydration and re-solvation of the surface by the next solvent are not too high.

The adsorption kinetics of particle adsorption may operate in different regimes, diffusion limited, activation energy limited or a combination of both. Therefore, it is expected that the decrease in IFT vs. time is slower for larger particles as compared to the smaller ones. Furthermore, according to the time evolution of the interfacial tension, the adsorption is characterised by three adsorption stages, depicted in Fig. 4.7: (I) the free diffusion of some particles to the interface (II) continuous adsorption of Janus particles to form domains at the interface, and (III) particle packing and rearrangement in compact domains/islands [41, 44].
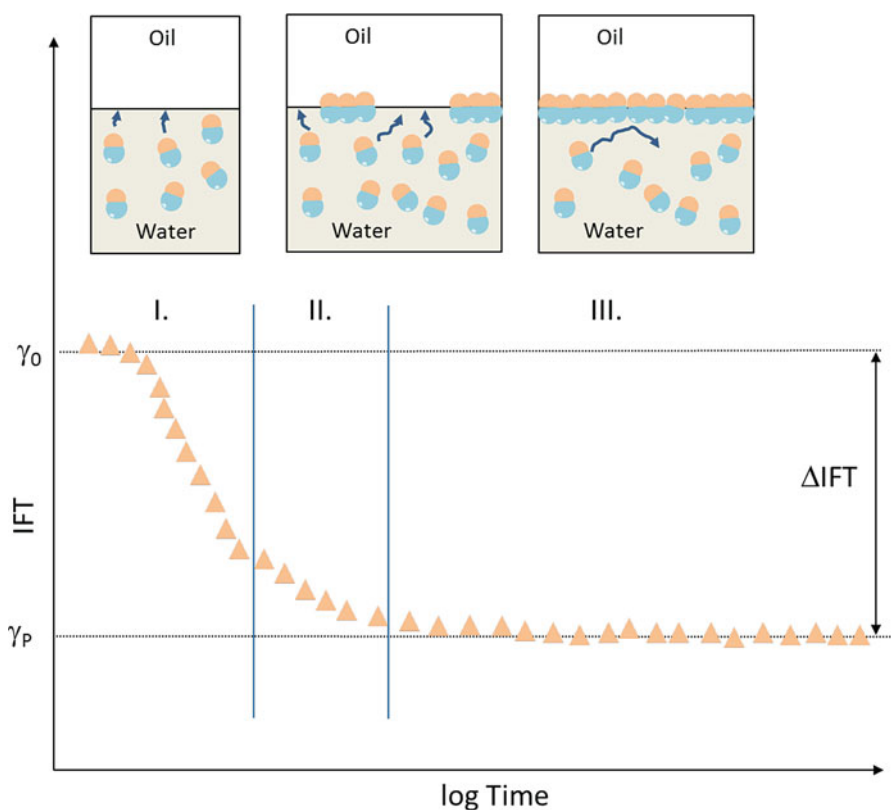
Fig. 4.7 Cartoon depicting the time evolution of the IFT and the three main stages of JPs adsorption: (I) JPs adsorb at a pristine oil–water interface, the diffusion from bulk-to-surface may be the limiting step, but also a large activation energy barrier to adsorption, (II) continuous adsorption of JPs at the interface and formation of domains and 2D islands and (III) full occupation of the interface by JPs, particle–particle repulsive interactions contribute to increasing the energy barrier to adsorption and interfacial re-organisation of the monolayer

The magnitude of ΔIFT, which is the distance between the starting value at $t = 0$ and t_{plateau} at which IFT does not decrease anymore, Fig. 4.7, indicates how effective the JPs are at lowering the interfacial tension. The magnitude of ΔIFT encompasses several phenomena, such as the ability of the particles to pack in a compact monolayer, surface and interfacial energy of the particles with both phases and the particle–particle lateral interactions. Hypothetically, the JPs can lower the IFT to almost zero if their interfacial energy with both phases is zero, perfect affinity for each lobe for the oil and water phases, and have the ability to pack compactly leaving no free oil–water interface. It has been predicted [13] and experimentally demonstrated that JPs have a significantly higher ability to lower the IFT than the HPs [45, 46]. The reason of that is that JPs constituted of two parts can achieve better solvent-JP and water-JP compatibility (that translate in very low interfacial energies), which cannot be achieved in HPs. In the case of JPs not only the size but also the shape affects the ΔIFT. As the shape changes from sphere to disc and rod, Gao et al. [41] observed different adsorption kinetics, different packing behaviours and ultimately different ΔIFT values. For the three types of Janus particles with the same surface area, the ability to decrease the interfacial tension increases from Janus sphere to Janus disc to Janus rod. The particle-interface interaction has also been shown to play a role, for example, the particle with a large zeta potential seems to adsorb better at the interface due to an interfacial charge re-distribution due to the strong electric field of the particle that locally inverts the charge density of the air–water interface [47]. The way the JNPs can assemble at the oil–water interfaces can be affected by their aspect ratio, i.e. the geometrical packing parameter and by the polarity contrast, analogue to molecular surfactants.

4.5.1 Contact Angle and Interfacial Adsorption Energies of HPs vs. JPs

The adsorption of the JPs at interfaces can be treated purely thermodynamically, whereas only the initial and final states are taken into account regardless of the path the system takes. For example, the Gibbs free energy of JPs' adsorption at oil–water interface can be calculated by taking into account the free energy of the particle in one of the bulk phases as the initial state and the free energy of the particle at the interface between two phases. The difference between the two will be the Gibbs free energy of JPs' adsorption or minus desorption energy. For an HP this can be easily calculated, for example, at the air–water interface if we know its contact angle β with water, Fig. 4.8.

The free energy can be calculated for any particle simply by multiplying its interfacial energy also known as the energy density (mJ/m^2) by its exposed area to each liquid forming the interface and for the case in Fig. 4.8 the free energy at the interface is:
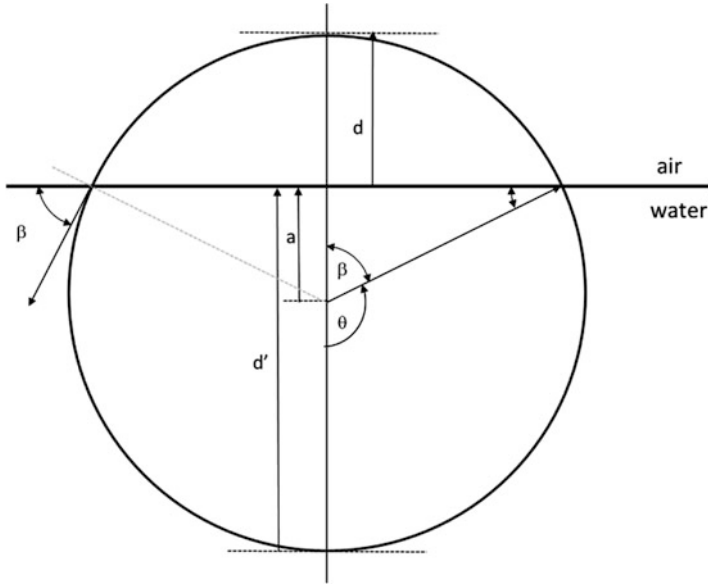
Fig. 4.8 Spherical particle adsorbed at the air–water interface. The contact angle with water β can be determined in two equivalent ways: (left) between the position of the air–water interface with the surface of the particle or (right) from the angle formed between the radius pointing at the three-phase line. The parameters a and d' are the immersion depth of the particle in water measured from the centre and apex of the particle, respectively, and d is the immersion of the particle in the second phase, air or oil

$$E_{\text{interface}} = \gamma_{(\text{HP,air})} A_{(\text{HP,air})} + \gamma_{(\text{HP,water})} A_{(\text{HP,water})}$$
$$+ \gamma_{(\text{air,water})} A_{(\text{circular base radius r})}. \tag{4.4}$$

The explicit expressions of the areas are:

$$A_{(\text{HP,air})} = 2\pi R(R-a) = 2\pi R[R - R\sin(\pi/2 - \beta)] = 2\pi R^2 (1 - \cos\beta) \tag{4.5}$$

$$A_{(\text{HP,water})} = 2\pi R(R+a) = 2\pi R[R + R\sin(\pi/2 - \beta)] = 2\pi R^2 (1 + \cos\beta) \tag{4.6}$$

$$A_{(\text{circular base radius r})} = \pi r^2 = \pi[R\cos(\pi/2 - \beta)]^2 = \pi R^2 \sin^2\beta, \tag{4.7}$$

where the last expression accounts for the area of the excluded air–water interfacial area.

Finally, the free energy of the HP at the interface is:

$$E_{\text{interface}} = \gamma_{(\text{HP,air})} 2\pi R^2 (1 - \cos\beta) + \gamma_{(\text{HP,water})} 2\pi R^2 (1 + \cos\beta)$$
$$+ \gamma_{(\text{air,water})} \pi R^2 \sin^2\beta. \tag{4.8}$$

The Gibbs free energy of a single HP completely immersed in water will be:

$$E_{\text{water}} = \gamma_{(\text{HP,water})} 4\pi R^2. \tag{4.9}$$

Therefore, the total interfacial adsorption energy only as a function of the contact angle β will be:

$$E_{\text{water}} - E_{\text{interface}} = \gamma_{(\text{HP,air})} 2\pi R^2 (1 + \cos\beta) - \gamma_{(\text{HP,water})} 2\pi R^2 (1 + \cos\beta)$$
$$- \gamma_{(\text{air,water})} \pi R^2 \sin^2\beta. \tag{4.10}$$

Pieranski [48] was among the pioneers to attempt calculating the particle energies at interfaces and the equations proposed were as a function of the HPs immersion depth "a", Fig. 4.8, which is the distance from the centre of the particle to the interface. This can obviously also be determined directly without the need to measure the contact angle directly from SEM of cryogenised particles trapped at interfaces [49]. The above expression as a function of "a" would be:

$$E_{\text{interface}} = \gamma_{(\text{Particle,air})} 2\pi R(R - a) + \gamma_{(\text{Particle,water})} 2\pi R(R + a)$$
$$+ \gamma_{(\text{air,water})} \pi (R^2 - a^2), \tag{4.11}$$

which after rearrangement becomes:

$$E_{\text{interface}} = \gamma_{(\text{Particle,air})} 2\pi R^2 (1 - a/R) + \gamma_{(\text{Particle,water})} 2\pi R^2 (1 + a/R)$$
$$+ \gamma_{(\text{air,water})} \pi R^2 [1 - (a/R)^2]. \tag{4.12}$$

The depth a is related to the interfacial tension via the Young–Dupré contact angle:

$$\cos\beta = \frac{a}{R} = \frac{\gamma_{(\text{HP,air})} \pm \gamma_{(\text{HP,water})}}{\gamma_{(\text{HP,water})}}. \tag{4.13}$$

The sign in parenthesis is the negative for $\beta < 90°$ and positive for $\beta > 90°$.

Very often in different works one finds the following expression as the energy with which a small particle of radius R is held at the air–water or oil–water interfaces[50]:

$$E_{\text{interface}} = \gamma_{(\text{air,water})} \pi R^2 [1 \pm \cos\beta]^2, \tag{4.14}$$

where the sign in parenthesis is the negative for $\beta < 90°$ and positive for $\beta > 90°$. This form of the last equation results from inserting the expression of $\cos\beta$ in Eq. (4.13), defined by the Young–Dupré expression, into the $E_{\text{interface}}$ expression Eq. (4.11) obtaining[51]:

$$E_{\text{interface}} = \gamma_{(\text{HP,air})} 2\pi R^2 (1 - \cos\beta) + \gamma_{(\text{HP,water})} 2\pi R^2 (1 + \cos\beta)$$

$$+ \gamma_{(\text{air,water})} \pi R^2 \sin^2\beta$$

$$= 2\pi R^2 \left[\gamma_{(\text{HP,air})} + \gamma_{(\text{HP,water})} + \cos\beta (\gamma_{(\text{HP,water})} - \gamma_{(\text{HP,air})}) \right]$$

$$+ \gamma_{(\text{air,water})} \pi R^2 \sin^2\beta$$

$$= 2\pi R^2 \left[\gamma_{(\text{HP,air})} + 2\gamma_{(\text{HP,water})} - \gamma_{(\text{HP,water})} - \gamma_{(\text{air,water})} \cos^2\beta \right]$$

$$+ \gamma_{(\text{air,water})} \pi R^2 \sin^2\beta$$

$$= 4\pi R^2 \gamma_{(\text{HP,water})} + 2\pi R^2 \left[\gamma_{(\text{air,water})} \cos\beta - \gamma_{(\text{air,water})} \cos^2\beta \right]$$

$$+ \gamma_{(\text{air,water})} \pi R^2 \sin^2\beta. \tag{4.15}$$

Keeping in mind that $\sin^2\beta = 1 - \cos^2\beta$,

$$E_{\text{interface}} = 4\pi R^2 \gamma_{(\text{Particle,water})} - \pi R^2 \gamma_{(\text{air,water})}$$

$$\times \left[1 - 2\cos\beta + 2\cos^2\beta - \cos^2\beta \right]$$

$$= 4\pi R^2 \gamma_{(\text{Particle,water})} - \pi R^2 \gamma_{(\text{air,water})} (1 - \cos\beta)^2, \tag{4.16}$$

where the first term in the last equation is the interfacial energy of a sphere completely immersed in water; therefore, the last term is the change in interfacial energy of the particle attached to the air–water interface, i.e. the final state. For example, if $\gamma_{(\text{air,water})} = 75 \, \text{mJ/m}^2$ and $R = 1 \, \mu\text{m}$ and $\beta = 90°$, then the energy holding the particle at the interface at room temperature would be $2.4 \times 10^{-13} \, \text{J} \approx 5.7 \times 10^7 \, \text{kT}$, where $1 \, \text{kT} = 4.114 \times 10^{-21} \, \text{J}$ at 298 K.

In order to calculate the Gibbs free energy of JPs adsorption at air–water interface, consisting of two hemispheres, one apolar (A) and one polar (P), one needs to calculate the energy difference between the particle entirely immersed in water and that adsorbed at air–water interface. This can be done following strictly the Ondarçuhu [12] nomenclature, which assumes a perfectly spherical JP and its adsorption at the interface occurs via partial dehydration of the surface of one lobe, as depicted in Fig. 4.9.

A. Case of partial de-wetting of the A-lobe, $\theta > \alpha$ and the general case $\alpha \neq \pi/2$.

In order to solve this, the expression of the energy for each interface must be found. Next, we find the expressions of $E_{(\text{A,air})}$, $E_{(\text{A,water})}$, $E_{(\text{P,water})}$ and $E_{(\text{air,water})}$ as a function of contact angle,

$$E_{(\text{A,air})} = \gamma_{(\text{A,air})} A_{(\text{A,air})} = \gamma_{(\text{A,air})} 2\pi R^2 (1 + \cos\theta), \tag{4.17}$$
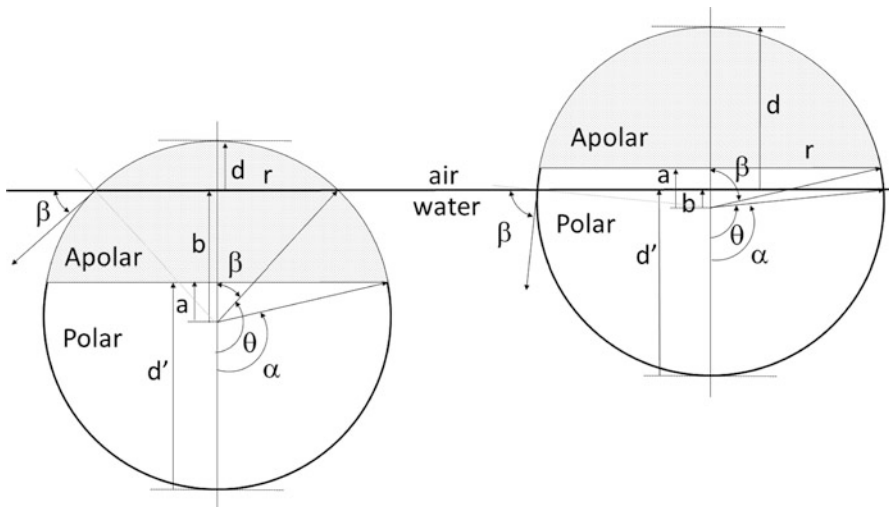
Fig. 4.9 A perfectly spherical JP adsorbed at the oil–water interface. (Left) Case of partial de-wetting of the A-lobe, for $\theta > \alpha$ and the general case $\alpha \neq \pi/2$. (Right) Case of partial de-wetting of the P-lobe, $\theta < \alpha$ and the general case $\alpha \neq \pi/2$

where the area is given by

$$
\begin{aligned}
A_{(A,\text{air})} &= 2\pi R d = 2\pi R(R-b) \\
&= 2\pi R^2[1 - \sin(\pi/2 - \beta)] = 2\pi R^2[1 - \sin(\pi/2 - \pi + \theta)] \\
&= 2\pi R^2[1 - \sin(-\pi/2 + \theta)] = 2\pi R^2[1 + \sin(\pi/2 - \theta)] \\
&= 2\pi R^2(1 + \cos\theta),
\end{aligned} \tag{4.18}
$$

and $\sin(-\pi/2 + \theta) = -\cos\theta$

$$
E_{(A,\text{water})} = \gamma_{(A,\text{water})} A_{(A,\text{water})} = \gamma_{(A,\text{water})} 2\pi R^2(\cos\alpha - \cos\theta), \tag{4.19}
$$

where

$$
b = R\sin(-\pi/2 + \theta) = -R\sin(\pi/2 - \theta) = -R\cos\theta \tag{4.20}
$$

$$
a = R\sin(-\pi/2 + \alpha) = -R\sin(\pi/2 - \alpha) = -R\cos\alpha \tag{4.21}
$$

$$
A_{(A,\text{water})} = 2\pi R^2(\cos\alpha - \cos\theta). \tag{4.22}
$$

The surface area of the zone, excluding the top and bottom bases is: $A_{(A,\text{water})} = 2\pi R h$, where $h = b - a$ and is the height of the zone.

$$E_{(P,\text{water})} = \gamma_{(P,\text{water})} A_{(P,\text{water})} = \gamma_{(P,\text{water})} 2\pi R^2 (1 - \cos\alpha), \tag{4.23}$$

where the area is:

$$A_{(P,\text{water})} = 2\pi R d' = 2\pi R(R + a) = 2\pi R^2 (1 - \cos\alpha) \tag{4.24}$$

$$E_{(\text{air},\text{water})} = \gamma_{(\text{air},\text{water})} A_{(\text{circular base radius r})} = \gamma_{(\text{air},\text{water})} \pi R^2 \sin^2\theta. \tag{4.25}$$

Therefore, the total Gibbs free energy of the JP at the interface is:

$$
\begin{aligned}
E = 2\pi R^2 \Big[& \gamma_{(A,\text{air})}(1 + \cos\theta) + \gamma_{(A,\text{water})}(\cos\alpha - \cos\theta) \\
& + \gamma_{(P,\text{water})}(1 - \cos\alpha) - \gamma_{(\text{air},\text{water})} \frac{1}{2}\sin^2\theta \Big].
\end{aligned}
\tag{4.26}
$$

This equation has several limiting cases, for example, if the Janus lobe is a perfect hemisphere, then $\alpha = \pi/2$ and the above equation becomes:

$$
\begin{aligned}
E = 2\pi R^2 \Big[& \gamma_{(A,\text{air})}(1 + \cos\theta) - \gamma_{(A,\text{water})}\cos\theta + \gamma_{(P,\text{water})} \\
& - \gamma_{(\text{air},\text{water})} \frac{1}{2}\sin^2\theta \Big].
\end{aligned}
\tag{4.27}
$$

Also, if instead of the parameters α and θ we use instead only the contact angle β, where $\theta = \pi - \beta$, then the equation becomes:

$$
\begin{aligned}
E_{\text{interface}} = 2\pi R^2 \Big[& \gamma_{(A,\text{air})}(1 - \cos\beta) + \gamma_{(A,\text{water})}\cos\beta \\
& + \gamma_{(P,\text{water})} + \gamma_{(\text{air},\text{water})} \sin^2(\beta)/2 \Big].
\end{aligned}
\tag{4.28}
$$

B. Case of total de-wetting of the A-lobe and partial de-wetting of the lobe P, $\theta < \alpha$ and the general case $\alpha \neq \pi/2$.

$$E_{(A,\text{air})} = \gamma_{(A,\text{air})} A_{(A,\text{air})} = \gamma_{(A,\text{air})} 2\pi R^2 (1 + \cos\alpha), \tag{4.29}$$

where

$$
\begin{aligned}
A_{(A,\text{air})} &= 2\pi R(R - a) = 2\pi R \big[R - R\sin(\pi/2 - \beta) \big] \\
&= 2\pi R \big[R - R\sin(\pi/2 - \pi + \alpha) \big] \\
&= 2\pi R \big[R + R\sin(\pi/2 - \alpha) \big] = 2\pi R^2 (1 + \cos\alpha)
\end{aligned}
\tag{4.30}
$$

$$E_{(P,air)} = \gamma_{(P,air)} A_{(P,air)} = \gamma_{(P,air)} 2\pi R^2 (\cos\theta - \cos\alpha), \tag{4.31}$$

where

$$R - b = R - R\sin(\theta - \pi/2) = R + R\sin(\pi/2 - \theta) = R + R\cos(\theta) \tag{4.32}$$

$$R - a = R + R\sin(\pi/2 - \alpha) = R + R\cos(\alpha) \tag{4.33}$$

$$A_{(A,water)} = 2\pi R^2 (\cos\theta - \cos\alpha) \tag{4.34}$$

$$\begin{aligned} E_{(P,water)} &= \gamma_{(P,water)} 2\pi R^2 (1 - \cos\theta) \\ A_{(P,water)} &= 2\pi R d' = 2\pi R(R + b) = 2\pi R^2 (1 - \cos\theta) \end{aligned} \tag{4.35}$$

$$\begin{aligned} E_{(air,water)} &= \gamma_{(air,water)} A_{(circular\ base\ radius\ r)} = \gamma_{(air,water)} \pi R^2 \sin^2\theta \\ A_{(circular\ base\ radius\ r)} &= \pi r^2 = \pi R^2 \cos^2(\pi/2 - \pi + \theta) = \pi R^2 \sin^2\theta. \end{aligned} \tag{4.36}$$

Therefore, the total Gibbs free energy of the particle at the interface is:

$$\begin{aligned} E_{interface} = 2\pi R^2 \Big[&\gamma_{(A,air)}(1 + \cos\alpha) + \gamma_{(A,water)}(\cos\theta - \cos\alpha) \\ &+ \gamma_{(P,water)}(1 - \cos\theta) - \gamma_{(air,water)}(\sin^2\theta)/2 \Big]. \end{aligned} \tag{4.37}$$

The surface energy of the Janus particles located completely in air(or oil) $E_{air(oil)}$ or water E_{water} can be easily found by setting the angle β in the particle Gibbs free energy equations to 0° or 180°, respectively. Further, Binks and Fletcher [13] also suggested that the interfacial activity of the particle should be evaluated by the magnitude of its energy of interfacial detachment that should be equal to $E_{water} - E_{interface}$ but this can be debated. Because the above energies scale with R^2, this criterion of evaluating the interfacial activity of the particle cannot be used to compare particles of different size as the larger particle or even large particle, let's say a tennis ball would be the most interfacially active particle according to this framework of thinking. Instead we proposed that the measurable effects in the drop of the surface tension of the liquid or interfacial tension of oil–water should be instead used as criterion for estimating the interfacial activity of particles. In addition, this method is difficult to apply for JPs that are dumbbell shaped, for example, because it is difficult to keep track of the position of the long axis, and long axis tilt with the respect of surface normal, but in principle it can be done. However, determining accurately the contact angle on particles it is very difficult and therefore Ondarçuhu's model is difficult to apply in practice. Therefore, determining the Gibbs free energy of a particle at interface and especially of JPs is very difficult.

4.5.2 Inter-Particle Interaction at Interfaces vs. Lowering the Interfacial Tension

Once adsorbed at the oil–water and air–water interfaces the HPs are capable of interaction with other particles via electrostatic forces, van der Waals forces but also capillary action due to the interface deformation that lead to repulsive and attractive interactions. Because the latter is particularly true for the case of particles that strongly deform the interface, or very rough particles that pin the interface line, due to pinning the interface at a rough particle surface, for smooth colloids this is rarely the case. Capillary interactions occur especially when large particles, depending on their surface roughness, wettability by the liquid and buoyancy effect lead to interfacial deformation, by changing the local curvature of the interface. The effect of the capillary interaction can be attractive or repulsive depending on the local curvature of the interface [52]. The capillary interaction forces between particles bound at interfaces have been fully discussed by Kralchevsky and Nagayama [53]. This is also known as Cheerios effect, where the grains of cereals floating on the milk clump together exactly due to this effect, deformation of the milk–air interface.

On the other hand, the surface charge on the JPs' surface arises due to the ionisation of the charged groups in water. The interaction between particles is generally well described by the Derjaguin–Landau–Verwey–Overbeek (DLVO) theory. The expression for the overall electrostatic pair-potential interaction between two point charges at the air–water interface was first derived by Stillinger [54] using the Debye–Hückel theory. In non-aqueous solvents colloidal particles can also carry charge, but in non-aqueous solvents this is typically much less than in water due to lack of ionization of surface functional groups, therefore it is considered less important in the stabilization of colloids. Therefore, upon adsorption the part of the particle immersed in the water phase will remained charged, while the other in the non-polar solvent or air will be neutral or less charged which leads to an asymmetric formation of the double layer. This leads to the formation of a dipole with its vector oriented perpendicular at the interface. The parallel orientation of the dipolar interfacial vectors oriented in the same way leads to repulsion. Therefore the overall contribution to the interaction pair-potential $U(r)$ are the repulsive double-layer interactions at the short range and dipole–dipole repulsion at longer range [55]. The magnitude of the dipole–dipole interaction is critical for particle assembly and ordered 2-D crystal monolayer formation at the interface as noted by Pieranski [48]. Van der Waals interaction may also play a role but its effects are negligibly small compared to the electrostatic repulsion.

With respect to interfacial tension or surface tension modification by particles the adsorption of the HPs at the interface is expected to have some measurable effects. In a recent study [56] the interfacial activity of simple non-amphiphilic silica nanoparticles at air–water and hexadecane–water interface done with pendant drop tensiometry has shown that indeed simple homogeneous particles produce a notable effect in IFT drop upon interfacial adsorption. Silica HPs with most "favourable" wetting, close to 90° reach the interface, are able to produce the strongest effect on

the IFT drop. The magnitude in IFT drop is expected to be dependent on the bulk particle concentration. Much earlier, Okubo [57] has shown the same effect on PS nanoparticle, with most noticeable effect in IFT drop occurred when the particle concentration was large enough that crystallites formation was already noticeable in the bulk phase. Notable is also the work of Johnson et al. [58–60] that studied the effects of TiO_2 nanoparticle adsorption and found a similar dependence in IFT drop with increase in HPs concentration. A measurable drop in the IFT of an air–water or oil–water interface can occur as a consequence of the weakening of the cohesion forces in the top-most interfacial layer, as it is the case for surfactants possessing an alkyl tail which sticks out into the non-polar phase or air and is only able to weakly interact with the neighbouring adsorbed particles, thus weakening the cohesion and the IFT. Striolo et al. [61] have shown that the IFT decreases significantly when the surface coverage is large enough that repulsive HP–HP interactions are expected. The existence of strong inter-particle capillary interaction may lead to an increase in the observed IFT as observed by Johnson and Dong [59].

Similar behaviour is expected for JPs, however with some differences. If the JPs consist of the polar part and an apolar part decisive for their interfacial behaviour is the polarity contrast between the Janus lobes and the role these play in JP–JP interfacial interaction. Ignoring the interfacial deformation effects and excluding the capillary interactions, the interfacial activity determined by the ΔIFT can be more dramatic then say that observed for the HPs with the same size, surface properties and composition as each of the Janus lobe. As pointed out earlier the interfacial activity of the particles cannot be estimated solely by the interfacial adsorption/desorption Gibbs free energy parameter because this scales with R^2, which becomes ambiguous when comparing particles that differ in size. Instead we propose that the interfacial activity should be evaluated by the ability to decrease the IFT of an interface—this is Janus effect. The Janus effect has been demonstrated by Fernández-Rodríguez et al. [31] on PMMA/PtBMA JPs microparticles fabricated by electrohydrodynamic co-jetting method and by us on PDIPAEMA/PS JPs nanoparticles [62]. Yet, another example of enhanced interfacial activity of JPs compared to the constituting HPs is that of Glaser et al. [45] which observed a significant decrease in the IFT vs. time of Au/Fe_2O_3 JPs at hexane–water interface. The ability of JPs to adsorb at interfaces and lower the IFT may find important applications in oil recovery applications [63].

4.5.3 Activation and Adsorption Energies of JPs Spontaneously Adsorbing at Interfaces

The adsorption of particles at interfaces is mostly entropically driven, the overall free energy of the system decreases due to increase in the water entropy; the ordered water layer on the surface of the particles becomes free upon particle interfacial adsorption. The dehydration and re-solvation of the surface involves however some
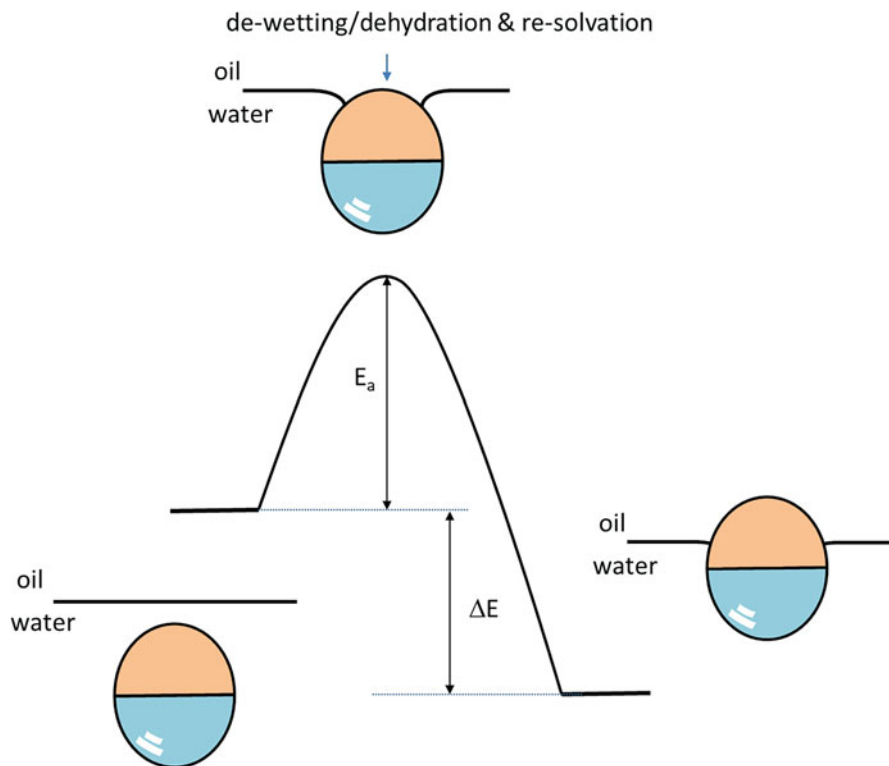
Fig. 4.10 Cartoon depicting the adsorption energy ΔE and the activation energy E_a for interfacial adsorption of JP at the oil–water. The JPs are drawn with a hypothetical orientation, long axis perpendicular to the interface

energy costs and it is one of the factors contributing to the magnitude of the activation energy barrier, Fig. 4.10. Activation energy can also arise due to particle-interface electrostatic interactions, or between the incoming particles and already adsorbed particles at the interface.

The adsorption energies of JNPs at interfaces can be calculated by first measuring the contact angle of the JPs with the solvents from the two phases, adopting a geometric model and performing the calculations as shown in Sect. 4.5.1. For complex JP geometries such as dumbbell shape or disc shape, the contact angle with each liquid phase is much more difficult to determine because it greatly increases the complexity of the geometric model in Sect. 4.5.1, adding severe uncertainties mainly due to many possible orientations of particles at the interface, the exact value of the angle of the long axis of the particle with respect to the surface. A much simpler way is to directly calculate the adsorption energy from the IFT vs. time data using pendant drop tensiometry. In pendant drop tensiometry the IFT drop with time can be monitored at oil–water interface for a long time. Same measurements can be performed at the air–water interface but have the disadvantage of the liquid

evaporation leading to relatively shorter observation times. Such measurements are universally applicable to any interfacially active compound, for all types of particles and surfactants. The IFT vs. time curves data represent the starting point and opportunity to apply different kinetic models. The same kinetics models that apply to HPs [44] also apply to JPs without restrictions. The dynamic IFT measurement typically stops when ΔIFT remains constant over time, that is, a plateau equilibrium value of the interfacial tension, γ_p, has been reached, Fig. 4.7.

Bulk particle concentration can influence the magnitude of the ΔIFT until the interface becomes fully saturated. Determining the maximum ΔIFT achieved at the highest concentration of particles is an important parameter for calculating the interfacial adsorption energy of the particle. A typical evolution of the IFT vs. time function of concentration is given in Fig. 4.11 and corresponds to PS-PDIPAEMA/P(3-TSPM) JPs at heptane–water interface [62]. Notice that γ_p remains constant above a concentration of 10 mg/mL PS-PDIPAEMA/P(3-TSPM)-1 JPs meaning that the maximum ΔIFT was reached at this concentration. In addition,
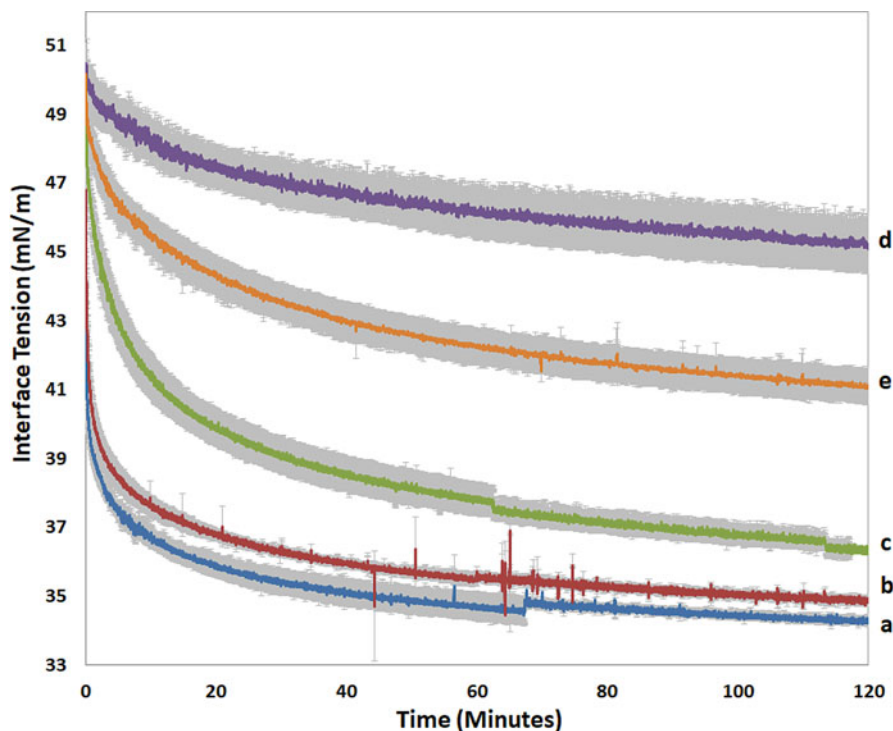
Fig. 4.11 IFT vs. time curves of the heptane–water interface in the presence of PS-PDIPAEMA/P(3-TSPM)-1 JPs at pH = 2: (**a**) 20 mg/mL, (**b**) 10 mg/mL, (**c**) 1 mg/mL, (**d**) 0.1 mg/mL and HNPs (**e**) at 10 mg/mL. Each data point is the average of three independent measurements and the error bars in grey represent the standard deviation. The data was acquired at 21 °C. Reprinted with permission from Ref. [62]. Copyright 2017 American Chemical Society

in the same figure the dynamic surface tension of JPs is compared to that of the HPs of the same composition and size as each of the Janus lobe and can be concluded that the latter are considerably less efficient than the JPs at lowering the IFT, in agreement with other similar findings of Fernández-Rodríguez et al.[31], Glaser et al. [45]. This demonstrates that the amphiphilicity of Janus particles enhances the interfacial activity of the particles.

Dinsmore et al. [64] proposed that the lowest γ_p, reached when the interface is fully saturated with particles, can be used to calculate the interfacial attachment energy ΔE:

$$\Delta E = -(\gamma_0 - \gamma_p)\pi R^2/\eta, \tag{4.38}$$

where γ_0 is the IFT for the initial concentration of particles adsorbed at the interface, Fig. 4.7, and R is the radius of the particles. Analysing the dynamic IFT measurement curves in Fig. 4.11 for the polymeric JPs adsorbing at the heptane–water interface, Wu and Honciuc [62] calculated energy of attachment ΔE using Eq. (4.38) and the obtained values are compared to the values obtained at heptane–water, toluene–water and air–water interfaces that are summarised in Table 4.2. Interestingly the ΔE values for the JPs are larger than those of HPs at the same interfaces within one order of magnitude, larger than those predicted by the calculations of Binks and Fletcher [13].

The *activation energy of adsorption* can be determined from the same IFT vs. time curves. As already mentioned the adsorption kinetics of any particle at interfaces could be diffusion controlled, energy barrier controlled or a combination of two [65–67]. The adsorption kinetics of HPs measured via pendant drop dynamic IFT measurements are typically modelled using Ward and Tordai theory [68], which considers that adsorption is controlled by the particle's concentration and bulk diffusivity followed by instantaneous adsorption at the interface. However, in the presence of an energy barrier, the adsorption at the interface is much slower than those predicted by purely diffusive models of Ward and Tordai. In order to account

Table 4.2 Activation energies of attachment of the PS-PDIPAEMA/P(3-TSPM) JPs and PS-PDIPAEMA HPs at toluene–water, heptane–water and air–water interfaces and their diffusivity, effective vs. actual

Interface	D_0 (m^2 s^{-1})	D_{eff} (m^2 s^{-1})	E_a (k_BT)	ΔE (k_BT)
JPs/toluene–water	1.65×10^{-12}	5.41×10^{-15}	5.8	-2.2×10^5
JPs/heptane–water	1.65×10^{-12}	6.24×10^{-15}	5.6	-2.9×10^5
JPs/air–water	1.65×10^{-12}	1.47×10^{-15}	7.1	-7.2×10^4
PDIPAEMA HPs/tol–water	4.94×10^{-12}	3.39×10^{-15}	7.3	-3.0×10^4
PDIPAEMA HPs/hep–water	4.94×10^{-12}	1.23×10^{-14}	6.0	-6.9×10^4
PPDIPAEMA-2 HPs/air–water	4.94×10^{-12}	1.83×10^{-15}	8.0	-2.0×10^4

Reprinted and adapted with permission from Ref. [62]. Copyright 2017 American Chemical Society

for this discrepancy Liggieri et al. [65] and Ravera et al. [66] proposed the effective diffusion model that includes an activation energy barrier. In other words not all the particles that arrive at the interface via diffusion also adsorb at the interface. Some particles that have a low kinetic energy are not able to overcome the potential barrier for surface adsorption and will diffuse back into the bulk, Fig. 4.7. The effective diffusion model enables the calculation of the activation energy barrier from the observed effective diffusion coefficient from the IFT vs. time data. The D_{eff} can be determined from the IFT vs. time data using the following equation [67]:

$$\gamma = \gamma_0 - 2N_A C_0 \Delta E \sqrt{\frac{D_{\text{eff}} t}{\pi}}, \tag{4.39}$$

where C_0 is the concentration of particles in bulk, γ_0 is the surface tension of the clean interface and ΔE is the attachment energy calculated with Eq. (4.38). By fitting the earlier portion of the IFT vs. $\sqrt{t}$ time curves one can calculate the D_{eff}. Fitting only the earlier portion of the curves is justified by the fact that the incoming particles meet a pristine interface in the first stage of adsorption, at a later time the electrostatic repulsion between the adsorbed and incoming particles dominates, Fig. 4.7 [67]. The obtained effective diffusion coefficient D_{eff} can be compared with the ones calculated from the Stokes–Einstein equation:

$$D_0 = \frac{k_B T}{6\pi \mu R}, \tag{4.40}$$

where μ is the viscosity of water and R is the hydrodynamic radius of the particle. The D_{eff} is typically much lower than the Stokes–Einstein diffusivity if an energy barrier is indeed present. Basavaraj et al. [67] obtained differences between D_{eff} vs. D_0 as large as three orders of magnitude for 10 nm silica particles at dodecane–water interface. The activation energy for attachment can be further calculated from the equation:

$$D_{\text{eff}} = D_0 \exp \left(\frac{-E_a}{k_B T} \right), \tag{4.41}$$

where E_a is the activation energy of attachment at interfaces. The calculated values of ΔE, γ_p, D_{eff} and D_0 and E_a for PS-PDIPAEMA/P(3-TSPM) JPs and the PS-PDIPAEMA HPs at three interfaces are compared in Table 4.2, whereas P(3-TSPM) HPs are not interfacially active. A quick inspection of the data shows that the D_{eff} effective diffusion coefficient is three orders of magnitude lower in all cases than for the Stokes diffusion coefficient calculated with Eq. (4.40), which can only be explained by the existence of an activation energy barrier. The E_a values are the largest for the air–water interface and the lowest for the adsorption at the heptane–water interface which can be explained in part by the good ability of heptane to "wet" and replace the water hydration layer from the JP surface, while at the air–water interface the high cost of JPs' surface dehydration remains uncompensated. Further, the value of ΔE for JPs than HPs, up to ten times at the heptane–water interface and up to three times at the air–water interfaces is larger than the three

times upper limit predicted by the calculations of Binks and Fletcher [13]. The reason for this discrepancy may lie in the shape of the particle, which is snowman type while Binks and Fletcher have treated a perfectly spherical shaped JP.

4.6 Pickering Emulsions: Arrested JPs at Interfaces

Emulsions are mixtures of two immiscible liquids, typically oil and water, that find many applications ranging from food, cosmetics, pharmaceuticals and enhanced oil recovery. The emulsions destabilise via coalescence and Ostwald ripening resulting in phase separation, therefore enhancing their stability and extending the shelf-life of emulsion-based products represents an important topic for research and development. Pickering emulsions are emulsions stabilised by particles and have been named after the British chemist and horticulturist S.U. Pickering who first discovered them in 1907. The particles adsorb at the interface between oil–water and prevent the formed droplets from coalescing. When producing Pickering emulsion typically external energy input is required in form of mechanical stirring or ultrasonication. One advantage of the Pickering emulsions as compared to standard surfactant emulsions is their stability. Pickering emulsions can be used in a variety of applications from, drug delivery, scaffolding materials for tissue and bone growth, environmentally responsive materials, catalysis [69]. Yang et al. gave a general description of Pickering emulsions and their applications [69].

A variety of homogeneous and asymmetric nanoparticles can be used for stabilising and forming Pickering emulsions. Particles are first dispersed in one of the phases, but typically in water, and then oil is added and then high shear forces are applied, either by ultrasonication, shaking or high-power stirring. For particles that exhibit good interfacial activity the external energy input can also be lower and gentle shaking by hand may suffice for producing emulsions. It is important to note that when external energy is applied via ultrasonication or shearing forces, particles acquire high kinetic energy, easily overcome the activation energy barrier to interfacial attachment as depicted in the cartoon in Fig. 4.10. Due to the energy input one of the phases becomes dispersed forming droplets whose interface is then "bombarded" by particles and becomes quickly saturated. The particles are irreversibly trapped at the interfaces, because the desorption energy is very high, some refers to this as arrested particles at the interfaces or arrested adsorption.

Depending on the affinity to one phase or the other, oil-in-water (o/w) or water-in-oil (w/o) emulsions can be obtained. The phase of the emulsion is determined by the particles' affinity to one phase or the other according to Finkle et al.[70] and similar to the Bancroft rules [71]. For example, hydrophobic carbon black particles are more likely to form w/o emulsions than the silica particles, due to their higher affinity to the apolar phase than to water [72]. Affinity of the particle to one of the phases translates into a preferred immersion depth into one phase or the other, changing in this way the curvature of the interface toward one phase or the other, as depicted in Fig. 4.12. Affinity of a particle to the interface has to do with its
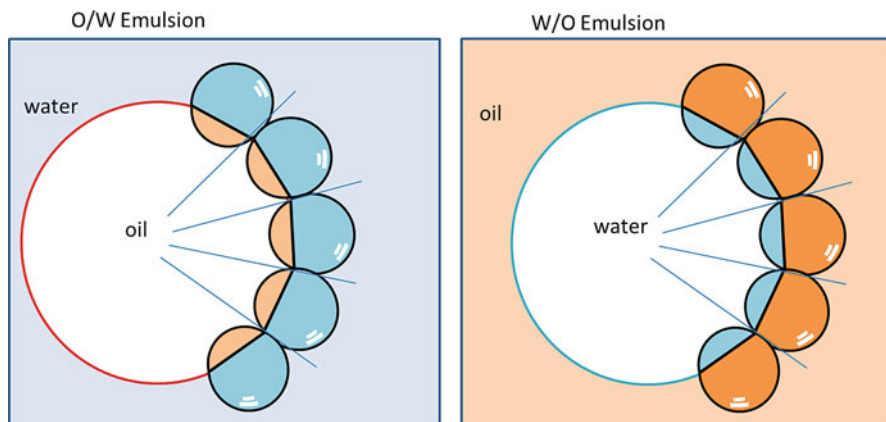
Fig. 4.12 Cartoon depicting the emulsion phase as function of the immersion depth (affinity) of a particle into the oil phase or the water phase (left) formation of o/w emulsions when the affinity of the particles is greater for water; (right) formation of w/o emulsion when the affinity of the particles is greater for oil

wettability, contact angle and eventually the immersion depth at the interface. If the immersion depth in one of the phases is stronger than the curvature of the interface will be such that the dispersed phase becomes the phase in which the particles are least immersed.

Why choosing JPs over HPs for Pickering emulsions? It has been demonstrated that the JPs are more interfacially active than the HPs due to their amphiphilicity. From the thermodynamic point of view the JPs stabilised emulsion are energetically more favourable than the HPs due to the positive line tension acting at the three-phase line oil–water–particle [73]. In addition, the surface polarity of HPs can be hard to control by surface chemical modification, often involving surface capping agents that are themselves surface active and do interfere in emulsification ability. It is for this reason why the surfactant-free JPs are more attractive than HPs in emulsification and other interfacial applications, because of the ability to precisely and gradually tune their overall polarity. Their surface energy can be varied by changing the aspect ratio between the lobes of different polarities to the desired conditions without using modifying agents like surfactants.

For example, a homologous series of five nano-sized PS/P(3-TSPM) JPs with different relative lobe sizes were tested for their emulsification ability of different volumetric ratios of heptane:water mixtures (heptane is a purely apolar liquid)[74]. Photographs of the emulsions obtained with these JPs series and the corresponding fluorescence microscopy images are presented in Fig. 4.13, whereby the top row depicts the SEM images of each particle in the homologous series; the first particle is PS HPs from which the second Janus lobe (brighter lobe) was generated, in addition the oil phase is fluorescent and the dark phase is water. The yellow line delimitates the boundary at which the emulsion phase inversion from w/o (top of the line) to o/w (bottom of the line) emulsion takes place. The horizontal yellow line depicts a transitional emulsion phase inversion that depends on the polarity of
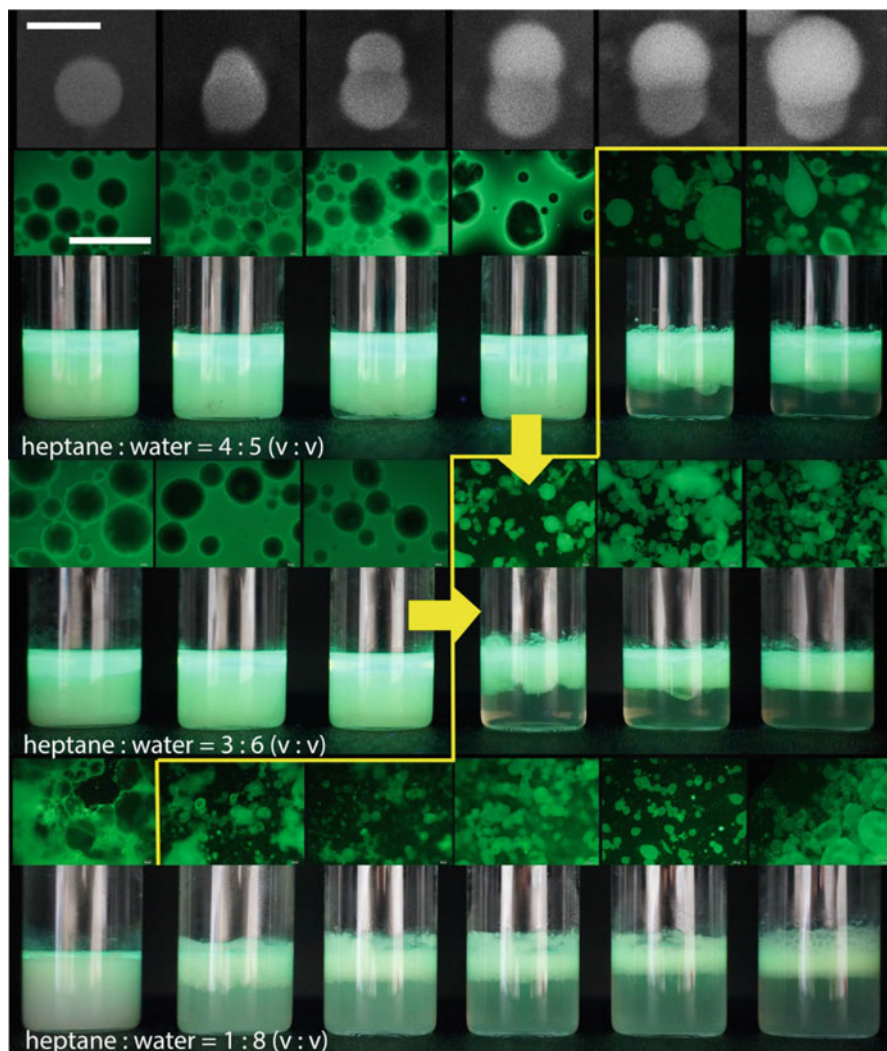
Fig. 4.13 Formulation—composition maps with photographs of emulsions in glass vials and their corresponding fluorescence microscopy images (scale bar is 400 nm) obtained with PS/P(3-TSPM) JPs. The top row depicts seed HPs and five PS/P(3-TSPM) JPs with increasing P(3-TSPM) lobe sizes (scale bar is 200 nm), while the subsequent three rows represent a different volumetric ratio of heptane to water and the six columns represent the emulsification results from each particle. The yellow line indicates the w/o and o/w emulsion phase boundary; the vertical arrow indicates the catastrophic and the horizontal the "static" transitional phase inversion. The fluorescent phase is the oil phase and the dark phase the water. Reprinted with permission from Ref. [1]. Copyright 2016 American Chemical Society

the particle, its affinity to one of the phases and eventually its immersion depth according to the cartoon in Fig. 4.12. This is the principle behind creating stimuli-responsive emulsions, discussed later. The vertical arrow indicates a catastrophic phase inversion that depends on the volume oil:water; when the ratio of one of the phases is considerably lower than the other phase, then the probability that this becomes the dispersed phase is higher. Note that the catastrophic phase inversion does not affect the particle immersion depth at the interface. From the results in Fig. 4.13 it is clear that the HPs (first column) are apolar, because they are only capable of forming w/o Pickering emulsions for all heptane:water ratios. A transitional emulsion phase inversion from w/o to o/w takes place in the middle of the homologous series, meaning that with the growth of the P(3-TSPM) the JPs become more polar and the affinity of the largest lobe JPs is greater toward water.

Other types of oils differing in their polarity and viscosity can be emulsified in water with JPs. Monomers, fragrant oils, polymers and organic solvents can be emulsified into Pickering emulsions. Further, Honciuc et al. [42] have shown that by changing the polarity of the emulsified oil the interfacial energy of the particles with the oil and water can be estimated. If monomers are used instead as oils, the Pickering emulsion can be subsequently polymerised resulting in solid-state polymers with nanostructured surfaces, see Fig. 4.14, and other advanced materials [42].
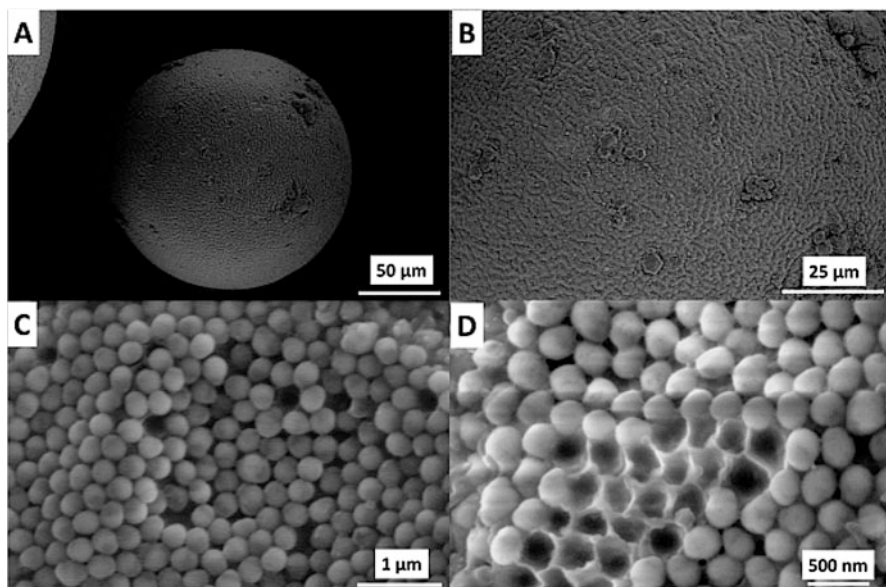

Fig. 4.14 (**a**) Polystyrene/JNP colloidosomes resulting from the polymerisation of a styrene-in-water emulsion obtained with PS/P(3-TSPM) JPs. Reprinted with permission from Ref. [42]. (**b**)-(**d**) zoomed in surface regions of the colloidosome, showing tight packing of the JPs monolayer. Copyright 2017 American Chemical Society

Stimuli-responsive Pickering emulsions can also be designed by using stimuli responsive particles. Upon adsorption of particles at interfaces the emulsion generated acquires the functionality of the populating particles. For example, Tu and Lee [38] have created stimuli-responsive Pickering emulsions from PS/PAA JPs which are capable of phase inversion due to deprotonation at high pH of the -COOH groups and thus polarity of the particle increases and becoming capable of forming o/w emulsions.

In a different example, Pickering emulsions stabilised by PDIPAEMA/P(3-TSPM) JPs it was also possible to induce an emulsion phase inversion by changing in situ the pH value of the water phase below and above the pKa value of the -NR$_3$ groups at the surface of the PDIPAEMA JP lobe, Fig. 4.15. When the pH is changed in situ and an already formed Pickering emulsion inverses its phase it is called a dynamic transitional emulsion inversion [72] in contrast to static transitional emulsion inversion that assumes the preparation of the emulsion at the given pH. Such pH-responsive Pickering emulsion could be employed in encapsulations and triggered release applications.

The use of Pickering emulsions in phase selective catalysis demonstrates the potential advantages and opportunities offered by the asymmetric architecture of the JPs. A conclusive example is that of Resasco et al. [75] which have produced JPs and loaded them with Pd nanoparticles selectively only on the hydrophobic side to produced Pd/JPs and non-selectively deposited everywhere to produce HPs. Next with these two types of particles they have created Pickering emulsions from decalin and water. The decalin phase contained benzaldehyde that was insoluble in
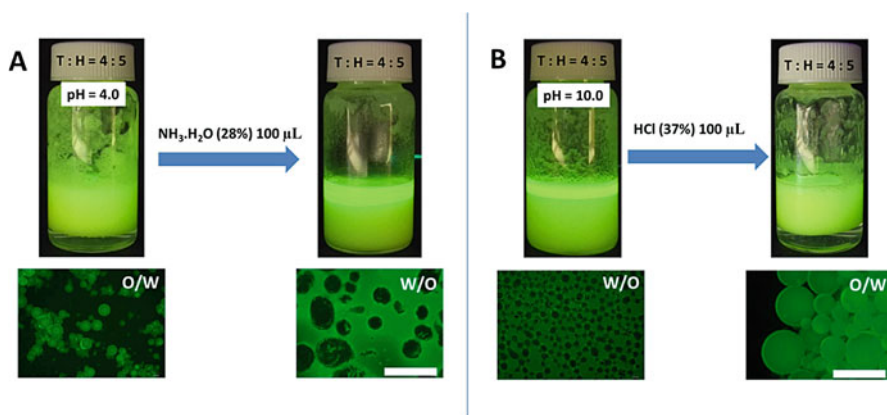
Fig. 4.15 Pickering emulsions stabilised by PDIPAEMA/P(3-TSPM) JPs showing dynamic emulsion phase inversion with the pH: (**a**) as prepared o/w Pickering emulsion (toluene:water = 4:5 ratio, pH = 4.0) changing to w/o after addition of base; (**b**) as prepared w/o Pickering emulsion (toluene:water = 4:5 ratio, pH = 10) changing to o/w after addition of acid. On top photographs of the vials containing the Pickering emulsions, with 0.1% hydrophobic dye and bottom the fluorescence microscopy images showing the corresponding Pickering emulsion type (scale bar = 200 μm). Reprinted with permission from Ref. [62]. Copyright 2017 American Chemical Society

water and the water phase contained glutaraldehyde that is insoluble in oil. Next, the two emulsions were hydrogenated and surprising results were obtained: when the catalyst contained Pd on both sides of the Janus particles, high conversion levels were obtained for both reactants, about 80% for glutaraldehyde in the water phase and 100% for benzaldehyde in the oil phase. However, when the catalyst had Pd selectively deposited on the hydrophobic side, the conversion of benzaldehyde was kept at 100%, while the conversion of glutaraldehyde decreased to 2%, demonstrating high phase selectivity, of JP stabilised Pickering emulsions. Similarly, Liu et al. [76] used Au nanoparticle modified SiO_2/PS-PDVB of the JPs as interfacial catalysts for the catalytic reduction of 4-nitroanisole to 4-aminoanisole.

4.7   Self-Assembly of Janus Particles

Similar to molecular surfactants JPs can also self-assemble into suprastructures. The key parameters behind the self-assembly of JPs are the right balance between the repulsive/attractive forces and their geometry that greatly influences the type of suprastructures formed [77, 78]. It is well known that HPs can assemble into colloidal crystals with iridescent appearance and find use in photonics [79, 80], electronics [81, 82], catalysis [83], (bio)sensing [84, 85], etc. In contrast, JPs can give rise to a larger variety of self-assembled suprastructures [86], such as trimmers [87], spherical micelles [88], capsules [89] and crystals [90], which can be of great importance for obtaining novel reconfigurable materials and assemblies at non-equilibrium also referred to as "active matter" that can perform different functions [91]. The different variety of suprastructures that can be formed arise from JPs anisotropy due to geometrical or topological constraints [92, 93], which affect their interaction and packing. JPs may find analogues in nature such as large proteins that exhibit polarity domains on their surface and exhibit anisotropy. Anisotropic proteins form self-assembly structures with precise morphology and specific functional role [94]. The ability of JPs to self-assembly into complex and regular structures that show unusual and reconfigurable properties [91] is a remarkable property and is one of the main driving motivations for further research in this area [93].

The particle–particle interaction drives the self-assembly of JPs in monophasic solvent, but their assembly can also be mediated by a minority liquid in a biphasic system, such as, for example, by placing spherical Au/SiO_2 JPs in a binary system of water/2,6-lutidine binary fluid leading to 2D and 3D clusters or zig-zag chains [95]. Other examples of JPs self-assemblies mediated by liquids in water/n-dodecane mixtures; in this case water was the minority liquid, mediating the self-assembly formation via capillary forces due to the formation of water bridges between particles. By progressively increasing the fraction water, a variety of structures from micelles, worm-like micelles and spherical emulsion droplets of spherical Au/SiO_2 JPs were obtained, Fig. 4.16 [96]. Eventually, when the minority liquid is large enough these transform into colloidosomes of Pickering emulsions, Fig. 4.16g–j;

Fig. 4.16 Optical microscope images showing α-dependence of the morphology in self-assembled structures, where α is the fraction of water (minority liquid) added in n-dodecane. (**a–i**) Optical microscope images of typical structures formed at respective α. (**a**) Random aggregate. (**b**) Small micelle-like cluster. (**c–e**) Rod-shaped micelle-like clusters. (**f**) Structure observed at a value of α where rod-shaped micelle-like clusters and spherical droplets coexist. (**g–i**) Spherical droplets in emulsions. (**i**) Hemispherical droplet attached to the bottom of the observation cell. (**j**) Magnified image of the framed region in (**i**). (**k**) Diagram of the α-range of the observed structures. The scale bars are 5 μm in (**a**) and (**b**), 10 μm in (**c**)–(**h**) and (**j**) and 50 μm in (**i**). Reprinted with permission from Ref. [96]. Copyright 2017 American Chemical Society
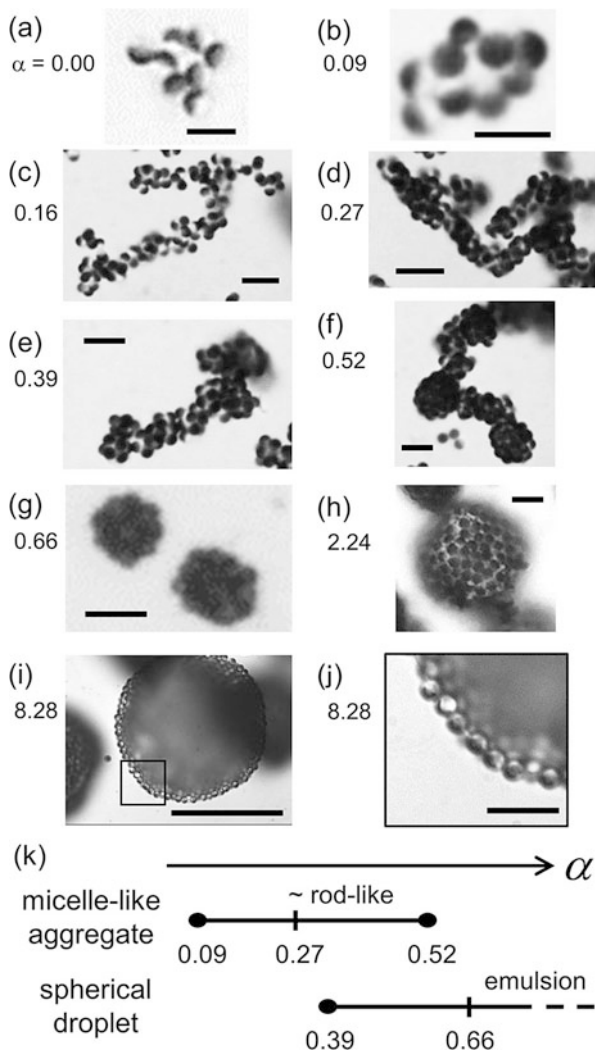
in addition the JPs are oriented with their polar lobe toward water. Hu et al. [97] showed that by further chemical alteration of the metallic side linkable Janus metal-organosilica particles capable of forming dimers and trimers can be created.

Because JPs can adsorb at the air–water interface, they can also act as gas bubble stabilisers and thus air bubbles can act as templates for the self-assembly. Gas bubbles and emulsions have similar properties, e.g. the gas can be thought of as a highly hydrophobic fluid. For example, Fujii et al. [98] obtained large mono-walled vesicles from Au/SiO$_2$ JPs; the orientation of JPs in the walls could be changed by chemical modification of the Au lobe with different polymers, PS, PPFBEM (Fig. 4.17).
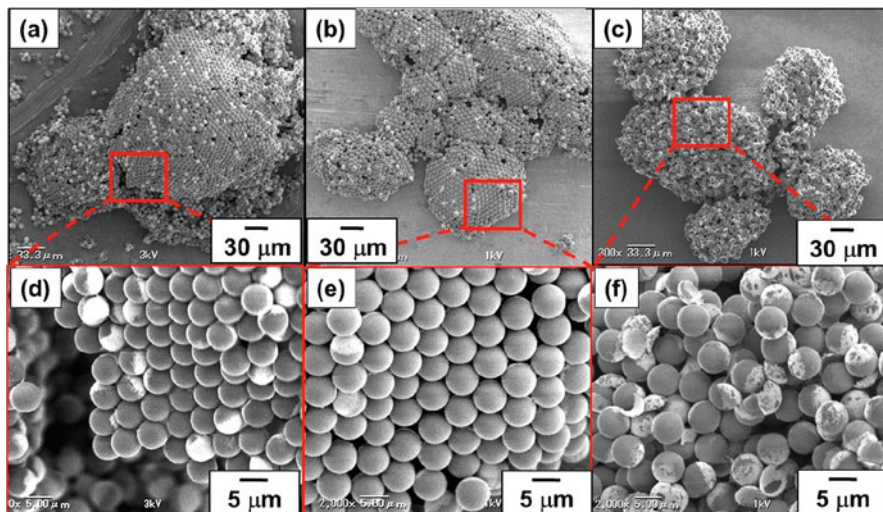
Fig. 4.17 SEM images of bubbles stabilised by the (**a, d**) Au-SiO$_2$, (**b, e**) PS-g-Au-SiO$_2$ and (**c, f**) PPFBEM-g-Au-SiO$_2$ Janus particles. Panels **d–f** are magnifications of panels **a–c**, respectively. Reprinted with permission from Ref. [98]. Copyright 2017 American Chemical Society

4.8 JP-Based Nanomotors

Self-propelled, active colloidal systems are of great fundamental interest with potential applications in nanomachineries, nanoscale assembly, catalysis and sensing [99]. Due to their asymmetry JPs possess the right architectures for making nanomotors [100] and the ways to power these externally have been extensively discussed by Shields and Velev [100]. For self-propulsion a motor needs fuel and in order to propel a Janus particle one side of it must be made apt for propelling the particles. One way this can be achieved is by making one lobe of the JPs from a metal that catalyses the decomposition of the H$_2$O$_2$ on its surface, such as Pt; the resulting decomposition products O$_2$ and H$_2$O act as propelling jet for the JPs. In this way the motion of the particle deviates from that of a pure Brownian motion and enhances the diffusivity of the particle in the bulk solution. The self-propelled JPs are also capable of transporting a cargo. Sanchez et al. [101] coated mesoporous silica nanoparticles on one side by evaporation of 2 nm thin Pt metal. The resulting JPs exhibited an enhanced diffusion coefficient of up to 100% and Rhodamine B could be loaded into the pores of the silica nanoparticles. The presence of H$_2$O$_2$ may limit however their application in vivo for drug delivery. Wang et al. [102] used a different fuel/metal system by deposition Ir-metal on one side of silica particles and using hydrazine (well-known monopropellant for rocket motors); N$_2$, H$_2$ and NH$_3$ molecules are generated at the Ir surface as a result the JP motor moves unidirectionally in the direction of the silica face. The group of Joseph Wang also showed that the capabilities of cargo transport of JP self-propelled motors are not
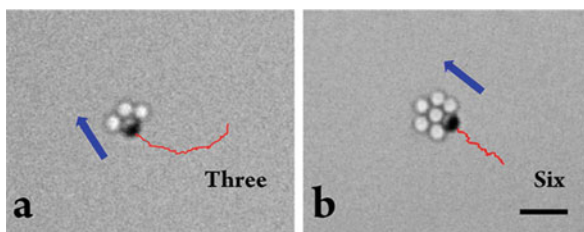
Fig. 4.18 Self-organised cargo loading. Time-lapse images (over 2 s) of the track lines of motor/nonmotor assemblies: transport of 3 (**a**) and 6 (**b**) nonmotor spheres (taken from SI Video 7). Scale bar, 5 μm. Reprinted with permission from Ref. [103]. Copyright 2013 American Chemical Society

only limited to small molecules but to other particles; using H_2O_2 fuel and Pt/SiO_2 JPs hydrophobised on the SiO_2 side with OTS, they could observe that JP motors can anchor HPs via hydrophobic interaction then transport them unidirectionally to a different location [103]. Impressively, one JP motor could transport up to six HPs. The mechanism of self-propulsion is well understood [104] and is achieved due to an asymmetric catalytic reaction occurring on the surface of the JPs. The role of the geometric shape in the unidirectional propulsion of JPs was also discussed [105]. By trapping Pt/SiO_2 JPs at the air/water surface Stocco et al. [106] were able to enhance the unidirectional motion of JPs as compared to bulk due to slowing down of the rotational diffusion at the interface and constraining it into a rotational well [36].

JPs' capabilities to self-assemble and unidirectional motion can be combined to achieve very unique operational functions, such as particle cargo applications [102, 103]. In Fig. 4.18a it is depicted the asymmetric cluster formation between a JP and three HPs; the three HPs are all attached to the alike JP lobe. The dark lobe catalyses a chemical decomposition reaction that is able to cargo the other particles and push them unidirectionally to a different location; one JP can transport up to 6 HPs, Fig. 4.18b.

4.9 Conclusions

Janus particles demonstrated a net superiority when compared to HPs in terms of interfacial behaviour and are therefore attractive for use in a plethora of interfacial applications. Stabilisation of Pickering emulsions, stabilisation of gas bubbles and foams are typical applications in which JPs have revealed their versatility. Further, due to their asymmetric architecture JPs open new horizons for particle applications. A few such possibilities have been already demonstrated, such as the self-assembly into reconfigurable suprastructures, paper display applications of bi-coloured JPs or cargo loading operation and transport of up to six particles by a single JP from point A to point B through chemically powered unidirectional motion. The future

application potential of the JPs appears limitless and further research may uncover even more extraordinary functions. The strength of these particles lies in the ability to carry different and often contrasting properties and functionalities on each of their lobes. These properties can be bulk-like properties or surface properties. For example, one can combine electric, magnetic and optic properties on each Janus lobes in addition to amphiphilicity, a surface property [6]. By doing this one can couple surface and bulk properties and combine them in surprising new ways. Never before, has the application potential of particles been more exciting than the one opened by the Janus particles.

References

1. D. Wu, J. Chew, A. Honciuc, Polarity reversal in homologous series of surfactant-free Janus nanoparticles: toward the next generation of amphiphiles. Langmuir **32**(25), 6376 (2016)
2. Y. Wang, Y. Wang, D. Breed, V. Manoharan, L. Feng, A. Hollingsworth, M. Weck, D. Pine, Colloids with valence and specific directional bonding. Nature **491**(7422), 51 (2012)
3. E. Passas-Lagos, F. Schüth, Amphiphilic Pickering emulsifiers based on mushroom-type Janus particles. Langmuir **31**(28), 7749 (2015)
4. J. Gong, X. Zu, Y. Li, W. Mu, Y. Deng, Janus particles with tunable coverage of zinc oxide nanowires. J. Mater. Chem. **21**(7), 2067 (2011)
5. A. Walther, X. André, M. Drechsler, V. Abetz, A. Müller, Janus discs. J. Am. Chem. Soc. **129**(19), 6187 (2007)
6. V. Mihali, A. Honciuc, Semiconductive materials with tunable electrical resistance and surface polarity obtained by asymmetric functionalization of Janus nanoparticles. Adv. Mater. Interfaces **4**(23), 1700914 (2017)
7. P. de Gennes, Soft matter. Rev. Mod. Phys. **64**(3), 645 (1992)
8. C. Casagrande, P. Fabre, E. Raphaël, M. Veyssié, "Janus beads": realization and behaviour at water/oil interfaces. Europhys. Lett. **9**(3), 251 (1989)
9. G. Burghard, U. Holtschimdt, G. Koerner, R. Gerd, Particles, modified at their surface by hydrophilic and hydrophobic groups, US patent US4715986A (1984)
10. G. Rossmy, in *Structure, Dynamics and Properties of Disperse Colloidal Systems*, ed. by H. Rehage, G. Peschel (Steinkopff, Darmstadt, 1998), pp. 17–26
11. Y.C. Chen, V. Dimonie, M. El-Aasser, Interfacial phenomena controlling particle morphology of composite latexes. J. Appl. Polym. Sci. **42**(4), 1049 (1991)
12. T. Ondarçuhu, P. Fabre, E. Raphaël, M. Veyssié, Specific properties of amphiphilic particles at fluid interfaces. J. Phys. France **51**(14), 1527 (1990)
13. B. Binks, P. Fletcher, Particles adsorbed at the oil–water interface: a theoretical comparison between spheres of uniform wettability and "Janus" particles. Langmuir **17**(16), 4708 (2001)
14. M. Linder, Hydrophobins: proteins that self assemble at interfaces. Curr. Opin. Colloid Interface Sci. **14**(5), 356 (2009)
15. T. Sarlin, T. Nakari-Setälä, M. Linder, M. Penttilä, A. Haikara, Fungal hydrophobins as predictors of the gushing activity of malt. J. Inst. Brew. **111**(2), 105 (2005)
16. D. Suzuki, H. Kawaguchi, Janus particles with a functional gold surface for control of surface plasmon resonance. Colloid Polym. Sci. **284**(12), 1471 (2006)
17. M. McConnell, M. Kraeutler, S. Yang, R. Composto, Patchy and multiregion Janus particles with tunable optical properties. Nano Lett. **10**(2), 603 (2010)
18. S. Ye, R. Carroll, Design and fabrication of bimetallic colloidal "Janus" particles. ACS Appl. Mater. Interfaces **2**(3), 616 (2010)
19. S. Jiang, Q. Chen, M. Tripathy, E. Luijten, K. Schweizer, S. Granick, Janus particle synthesis and assembly. Adv. Mater. **22**(10), 1060 (2010)

20. L. Hong, S. Jiang, S. Granick, Simple method to produce Janus colloidal particles in large quantity. Langmuir **22**(23), 9495 (2006)
21. D. Suzuki, S. Tsuji, H. Kawaguchi, Janus microgels prepared by surfactant-free Pickering emulsion-based modification and their self-assembly. J. Am. Chem. Soc. **129**(26), 8088 (2007)
22. K. Fujimoto, K. Nakahama, M. Shidara, H. Kawaguchi, Preparation of unsymmetrical microspheres at the interfaces. Langmuir **15**(13), 4630 (1999)
23. T. Skelhon, Y. Chen, S. Bon, Synthesis of "hard-soft" Janus particles by seeded dispersion polymerization. Langmuir **30**(45), 13525 (2014)
24. L. Bradley, K. Stebe, D. Lee, Clickable Janus particles. J. Am. Chem. Soc. **138**(36), 11437 (2016)
25. Y. Sun, F. Liang, X. Qu, Q. Wang, Z. Yang, Robust reactive Janus composite particles of snowman shape. Macromolecules **48**(8), 2715 (2015)
26. M. Hoffmann, Y. Lu, M. Schrinner, M. Ballauff, L. Harnau, Dumbbell-shaped polyelectrolyte brushes studied by depolarized dynamic light scattering. J. Phys. Chem. B **112**(47), 14843 (2008)
27. J.W. Kim, R. Larsen, D. Weitz, Synthesis of nonspherical colloidal particles with anisotropic properties. J. Am. Chem. Soc. **128**(44), 14374 (2006)
28. K. Lee, J. Yoon, J. Lahann, Recent advances with anisotropic particles. Curr. Opin. Colloid Interface Sci. **16**(3), 195 (2011)
29. S. Lone, I. Cheong, Fabrication of polymeric Janus particles by droplet microfluidics. RSC Adv. **4**(26), 13322 (2014)
30. T. Nisisako, T. Torii, T. Takahashi, Y. Takizawa, Synthesis of monodisperse bicolored Janus particles with electrical anisotropy using a microfluidic co-flow system. Adv. Mater. **18**(9), 1152 (2006)
31. M.Á. Fernández-Rodríguez, S. Rahmani, K. Chris, M.Á. Rodríguez-Valverde, M.Á. Cabrerizo-Vílchez, C.A. Michel, J. Lahann, R. Hidalgo-Álvarez, Synthesis and interfacial activity of PMMA/PtBMA Janus and homogeneous nanoparticles at water/oil interfaces. Colloids Surf. A Physicochem. Eng. Asp. **536**, 259 (2018)
32. K.H. Roh, D. Martin, J. Lahann, Triphasic nanocolloids. J. Am. Chem. Soc. **128**(21), 6796 (2006)
33. K.H. Roh, D. Martin, J. Lahann, Biphasic Janus particles with nanoscale anisotropy. Nat. Mater. **4**(10), 759 (2005)
34. R. Shah, J.W. Kim, D. Weitz, Janus supraparticles by induced phase separation of nanoparticles in droplets. Adv. Mater. **21**(19), 1949 (2009)
35. B. Liu, H. Möhwald, D. Wang, Synthesis of Janus particles via kinetic control of phase separation in emulsion droplets. Chem. Commun. **49**(84), 9746 (2013)
36. R. Deng, S. Liu, F. Liang, K. Wang, J. Zhu, Z. Yang, Polymeric Janus particles with hierarchical structures. Macromolecules **47**(11), 3701 (2014)
37. C. Sosa, R. Liu, C. Tang, F. Qu, S. Niu, M. Bazant, R. Prud'homme, R. Priestley, Soft multifaced and patchy colloids by constrained volume self-assembly. Macromolecules **49**(9), 3580 (2016)
38. F. Tu, D. Lee, Shape-changing and amphiphilicity-reversing Janus particles with pH-responsive surfactant properties. J. Am. Chem. Soc. **136**(28), 9999 (2014)
39. S. Jiang, S. Granick, Controlling the geometry (Janus balance) of amphiphilic colloidal particles. Langmuir **24**(6), 2438 (2008)
40. R. Pasquali, M. Taurozzi, C. Bregni, Some considerations about the hydrophilic-lipophilic balance system. Int. J. Pharm. **356**(1–2), 44 (2008)
41. H.M. Gao, Z.Y. Lu, H. Liu, Z.Y. Sun, L.J. An, Orientation and surface activity of Janus particles at fluid-fluid interfaces. J. Chem. Phys. **141**(13), 134907 (2014)
42. D. Wu, B. Binks, A. Honciuc, Modeling the interfacial energy of surfactant-free amphiphilic Janus nanoparticles from phase inversion in Pickering emulsions. Langmuir **34**(3), 1225 (2017)

43. C. Griffin, Calculation of HLB values of non-ionic surfactants. J. Soc. Cosmet. Chem. **5**, 249 (1954)
44. S. Kutuzov, J. He, R. Tangirala, T. Emrick, T. Russell, A. Böker, On the kinetics of nanoparticle self-assembly at liquid/liquid interfaces. Phys. Chem. Chem. Phys. **9**(48), 6351 (2007)
45. N. Glaser, D. Adams, A. Böker, G. Krausch, Janus particles at liquid-liquid interfaces. Langmuir **22**(12), 5227 (2006)
46. M.A. Fernandez-Rodriguez, Y. Song, M.Á. Rodríguez-Valverde, S. Chen, M.A. Cabrerizo-Vilchez, R. Hidalgo-Alvarez, Comparison of the interfacial activity between homogeneous and Janus gold nanoparticles by pendant drop tensiometry. Langmuir **30**(7), 1799 (2014)
47. A. Beloqui Redondo, I. Jordan, I. Ziazadeh, A. Kleibert, J. Giorgi, H. Wörner, S. May, Z. Abbas, M. Brown, Nanoparticle-induced charge redistribution of the air-water interface. J. Phys. Chem. C **119**(5), 2661 (2015)
48. P. Pieranski, Two-dimensional interfacial colloidal crystals. Phys. Rev. Lett. **45**(7), 569 (1980)
49. L. Isa, F. Lucas, R. Wepf, E. Reimhult, Measuring single-nanoparticle wetting properties by freeze-fracture shadow-casting cryo-scanning electron microscopy. Nat. Commun. **2**, 438 (2011)
50. B. Binks, S. Lumsdon, Effects of oil type and aqueous phase composition on oil-water mixtures containing particles of intermediate hydrophobicity. Phys. Chem. Chem. Phys. **2**(13), 2959 (2000)
51. S. Levine, B. Bowen, S. Partridge, Stabilization of emulsions by fine particles II. Capillary and van der Waals forces between particles. Colloids Surf. **38**(2), 345 (1989)
52. N. Vassileva, D. van den Ende, F. Mugele, J. Mellema, Capillary forces between spherical particles floating at a liquid-liquid interface. Langmuir **21**(24), 11190 (2005)
53. P. Kralchevsky, K. Nagayama, Capillary interactions between particles bound to interfaces, liquid films and biomembranes. Adv. Colloid Interface Sci. **85**(2–3), 145 (2000)
54. F. Stillinger, Interfacial solutions of the Poisson-Boltzmann equation. J. Chem. Phys. **35**(5), 1584 (1961)
55. O. Deshmukh, D. van den Ende, M. Stuart, F. Mugele, M. Duits, Hard and soft colloids at fluid interfaces: adsorption, interactions, assembly & rheology. Adv. Colloid Interface Sci. **222**, 215 (2015)
56. Y. Zhang, S. Wang, J. Zhou, R. Zhao, G. Benz, S. Tcheimou, J. Meredith, S. Behrens, Interfacial activity of nonamphiphilic particles in fluid-fluid interfaces. Langmuir **33**(18), 4511 (2017)
57. T. Okubo, Surface tension of structured colloidal suspensions of polystyrene and silica spheres at the air-water interface. J. Colloid Interface Sci. **171**(1), 55 (1995)
58. L. Dong, D. Johnson, The study of the surface tension of charge-stabilized colloidal dispersions. J. Dispers. Sci. Technol. **25**(5), 575 (2005)
59. L. Dong, D. Johnson, Surface tension of charge-stabilized colloidal suspensions at the water-air interface. Langmuir **19**(24), 10205 (2003)
60. K. Casson, D. Johnson, Surface-tension-driven flow due to the adsorption and desorption of colloidal particles. J. Colloid Interface Sci. **242**(2), 279 (2001)
61. X.C. Luu, J. Yu, A. Striolo, Nanoparticles adsorbed at the water/oil interface: coverage and composition effects on structure and diffusion. Langmuir **29**(24), 7221 (2013)
62. D. Wu, A. Honciuc, Design of Janus nanoparticles with pH-triggered switchable amphiphilicity for interfacial applications., ACS Appl. Nano Mater. **1**(1), 471 (2017)
63. B. Peng, L. Zhang, J. Luo, P. Wang, B. Ding, M. Zeng, Z. Cheng, A review of nanomaterials for nanofluid enhanced oil recovery. RSC Adv. **7**(51), 32246 (2017)
64. K. Du, E. Glogowski, T. Emrick, T. Russell, A. Dinsmore, Adsorption energy of nano- and microparticles at liquid-liquid interfaces. Langmuir **26**(15), 12518 (2010)
65. L. Liggieri, F. Ravera, A. Passerone, A diffusion-based approach to mixed adsorption kinetics. Colloids Surf. A Physicochem. Eng. Asp. **114**, 351 (1996)
66. F. Ravera, L. Liggieri, A. Steinchen, Sorption kinetics considered as a renormalized diffusion process. J. Colloid Interface Sci. **156**(1), 109 (1993)

67. V. Dugyala, J. Muthukuru, E. Mani, M. Basavaraj, Role of electrostatic interactions in the adsorption kinetics of nanoparticles at fluid-fluid interfaces. Phys. Chem. Chem. Phys. **18**(7), 5499 (2016)
68. A. Ward, L. Tordai, Time-dependence of boundary tensions of solutions I. The role of diffusion in time-effects. J. Chem. Phys. **14**(7), 453 (1946)
69. Y. Yang, Z. Fang, X. Chen, W. Zhang, Y. Xie, Y. Chen, Z. Liu, W. Yuan, An overview of Pickering emulsions: solid-particle materials, classification, morphology, and applications. Front. Pharmacol. **8**, 287 (2017)
70. P. Finkle, H. Draper, J. Hildebrand, The theory of emulsification. J. Am. Chem. Soc. **45**(12), 2780 (1923)
71. W. Bancroft, *Applied Colloid Chemistry*, 1st edn. (McGraw-Hill Book Co., New York, 1921)
72. A. Kumar, S. Li, C.M. Cheng, D. Lee, Recent developments in phase inversion emulsification. Ind. Eng. Chem. Res. **54**(34), 8375 (2015)
73. R. Aveyard, Can Janus particles give thermodynamically stable Pickering emulsions? Soft Matter **8**(19), 5233 (2012)
74. J. Israelachvili, in *Intermolecular and Surface Forces: Revised* (Academic, Amsterdam, 2011), pp. 415–467
75. J. Faria, M. Ruiz, D. Resasco, Phase-selective catalysis in emulsions stabilized by Janus silica-nanoparticles. Adv. Synth. Catal. **352**, 2359 (2010)
76. Y. Liu, J. Hu, X. Yu, X. Xu, Y. Gao, H. Li, F. Liang, Preparation of Janus-type catalysts and their catalytic performance at emulsion interface. J. Colloid Interface Sci. **490**, 357 (2017)
77. Y. Liu, W. Li, T. Perez, J. Gunton, G. Brett, Self-assembly of Janus ellipsoids. Langmuir **28**(1), 3 (2012)
78. W. Li, J. Gunton, Self-assembly of Janus ellipsoids II: Janus prolate spheroids. Langmuir **29**(27), 8517 (2013)
79. S.H. Kim, S. Lee, S.M. Yang, G.R. Yi, Self-assembled colloidal structures for photonics. NPG Asia Mater. **3**(1), 25 (2011)
80. A. Yethiraj, J. Thijssen, A. Wouterse, A. van Blaaderen, Large-area electric-field-induced colloidal single crystals for photonic applications. Adv. Mater. **16**(7), 596 (2004)
81. J. Anker, W. Hall, O. Lyandres, N. Shah, J. Zhao, R. Van Duyne, Biosensing with plasmonic nanosensors. Nat. Mater. **7**(6), 442 (2008)
82. C. Fenzl, T. Hirsch, O. Wolfbeis, Photonic crystals for chemical sensing and biosensing. Angew. Chem. Int. Ed. **53**(13), 3318 (2014)
83. E. Ortel, S. Sokolov, C. Zielke, I. Lauermann, S. Selve, K. Weh, B. Paul, J. Polte, R. Kraehnert, Supported mesoporous and hierarchical porous Pd/TiO2 catalytic coatings with controlled particle size and pore structure. Chem. Mater. **24**(20), 3828 (2012)
84. J. Anker, W. Hall, O. Lyandres, N. Shah, J. Zhao, R. Van Duyne, Biosensing with plasmonic nanosensors. Nat. Mater. **7**(6), 442 (2008)
85. C. Fenzl, T. Hirsch, O. Wolfbeis, Photonic crystals for chemical sensing and biosensing. Angew. Chem. Int. Ed. **53**(13), 3318 (2014)
86. S. Glotzer, M. Solomon, Anisotropy of building blocks and their assembly into complex structures. Nat. Mater. **6**, 557 (2007)
87. H. Hu, F. Ji, Y. Xu, J. Yu, Q. Liu, L. Chen, Q. Chen, P. Wen, Y. Lifshitz, Y. Wang, et al., Reversible and precise self-assembly of Janus metal-organosilica nanoparticles through a linker-free approach. ACS Nano **10**(8), 7323 (2016)
88. D. Kraft, R. Ni, F. Smallenburg, M. Hermes, K. Yoon, D. Weitz, A. van Blaaderen, J. Groenewold, M. Dijkstra, W. Kegel, Surface roughness directed self-assembly of patchy particles into colloidal micelles. Proc. Natl. Acad. Sci. **109**(27), 10787 (2012)
89. C. Evers, J. Luiken, P. Bolhuis, W. Kegel, Self-assembly of microcapsules via colloidal bond hybridization and anisotropy. Nature **534**(7607), 364 (2016)
90. E. Ducrot, M. He, G.R. Yi, D. Pine, Colloidal alloys with preassembled clusters and spheres. Nat. Mater. **16**, 652 (2017)
91. J. Zhang, S. Granick, Natural selection in the colloid world: active chiral spirals. Faraday Discuss. **191**, 35 (2016)

92. S. Sacanna, M. Korpics, K. Rodriguez, L. Colón-Meléndez, S.H. Kim, D. Pine, G.R. Yi, Shaping colloids for self-assembly. Nat. Commun. **4**, 1688 (2013)
93. V. Manoharan, Colloidal matter: Packing, geometry, and entropy. Science **349**(6251), 1253751 (2015)
94. J. Gunton, A. Shiryayev, D. Pagan, *Protein Condensation: Kinetic Pathways to Crystallization and Disease* (Cambridge University Press, Cambridge, 2007)
95. C. Yu, J. Zhang, S. Granick, Selective Janus particle assembly at tipping points of thermally-switched wetting. Angew. Chem. Int. Ed. **53**(17), 4364 (2014)
96. T. Noguchi, Y. Iwashita, Y. Kimura, Dependence of the internal structure on water/particle volume ratio in an amphiphilic Janus particle-water-oil ternary system: from micelle-like clusters to emulsions of spherical droplets. Langmuir **33**(4), 1030 (2017)
97. H. Hu, F. Ji, Y. Xu, J. Yu, Q. Liu, L. Chen, Q. Chen, P. Wen, Y. Lifshitz, Y. Wang, et al., Reversible and precise self-assembly of Janus metal-organosilica nanoparticles through a linker-free approach. ACS Nano **10**(8), 7323 (2016)
98. S. Fujii, Y. Yokoyama, S. Nakayama, M. Ito, S. Yusa, Y. Nakamura, Gas bubbles stabilized by Janus particles with varying hydrophilic-hydrophobic surface characteristics. Langmuir **34**(3), 933 (2017)
99. K. Dey, F. Wong, A. Altemose, A. Sen, Catalytic motors—quo vadimus? Curr. Opin. Colloid Interface Sci. **21**, 4 (2016)
100. C. Shields, O. Velev, The evolution of active particles: toward externally powered self-propelling and self-reconfiguring particle systems. Chem **3**(4), 539 (2017)
101. X. Ma, K. Hahn, S. Sanchez, Catalytic mesoporous Janus nanomotors for active cargo delivery. J. Am. Chem. Soc. **137**(15), 4976 (2015)
102. W. Gao, A. Pei, R. Dong, J. Wang, Catalytic iridium-based Janus micromotors powered by ultralow levels of chemical fuels. J. Am. Chem. Soc. **136**(6), 2276 (2014)
103. W. Gao, A. Pei, X. Feng, C. Hennessy, J. Wang, Organized self-assembly of Janus micromotors with hydrophobic hemispheres. J. Am. Chem. Soc. **135**(3), 998 (2013)
104. J. Gibbs, Y.P. Zhao, Autonomously motile catalytic nanomotors by bubble propulsion. Appl. Phys. Lett. **94**(16), 163104 (2009)
105. S. Michelin, E. Lauga, Geometric tuning of self-propulsion for Janus catalytic particles. Sci. Rep. **7**, 42264 (2017)
106. X. Wang, M. In, C. Blanc, M. Nobili, A. Stocco, Enhanced active motion of Janus colloids at the water surface. Soft Matter **11**(37), 7376 (2015)